UC-25
LBL-20512
c.1

Lawrence Berkeley Laboratory
UNIVERSITY OF CALIFORNIA

Materials & Molecular Research Division

RECEIVED
LAWRENCE
BERKELEY LABORATORY
JAN 31 1986
LIBRARY AND
DOCUMENTS SECTION

CHARACTERIZATION OF MACHINING DAMAGE IN GLASS

H. Tsai
(Ph.D. Thesis)

November 1985

For Reference

Not to be taken from this room

LBL-20512
c.1

Prepared for the U.S. Department of Energy under Contract DE-AC03-76SF00098

DISCLAIMER

This document was prepared as an account of work sponsored by the United States Government. While this document is believed to contain correct information, neither the United States Government nor any agency thereof, nor the Regents of the University of California, nor any of their employees, makes any warranty, express or implied, or assumes any legal responsibility for the accuracy, completeness, or usefulness of any information, apparatus, product, or process disclosed, or represents that its use would not infringe privately owned rights. Reference herein to any specific commercial product, process, or service by its trade name, trademark, manufacturer, or otherwise, does not necessarily constitute or imply its endorsement, recommendation, or favoring by the United States Government or any agency thereof, or the Regents of the University of California. The views and opinions of authors expressed herein do not necessarily state or reflect those of the United States Government or any agency thereof or the Regents of the University of California.

LBL-20512

CHARACTERIZATION OF MACHINING DAMAGE IN GLASS

Hsiao-chu Tsai
(Ph. D. Thesis)

Materials and Molecular Research Division
Lawrence Berkeley Laboratory
and
Department of Materials Sciences and
Mineral Engineering
University of California
Berkeley, California 94720

November 1985

This work was supported in part by the Director, Office of Energy Research, Office of Basic Energy Sciences, Materials Sciences Division of the U. S. Department of Energy under Contract No. DE-AC03-76SF00098 and by the Office of Naval Research under Contract N00014-81-K-0362.

CONTENTS

Page

ABSTRACT. v

1. Introduction 1

2. Background 2

2.1 Material Removal in Ceramic Machining. 2

2.2 Stress Field and Microfracture Beneath an Indenter under Normal and Horizontal Forces. 5

(a) Elastic Stress Field and Microfracture Geometry. 5

(b) Elastic/Plastic Indentation 6

2.3 Lateral Fracture Model of Material Removal 9

2.4 Indentation Plasticity in Brittle Surfaces 11

2.5 Crack Initiation in Elastic/Plastic Indentation. . . 12

2.6 Residual-Stress Effects in Strength Characteristics. 15

3. Experimental 21

4. Results. 23

4.1 Crack Length 23

4.2 Strengths. 24

4.3 Morphological Studies. 25

5. Discussion 25

5.1 The Reduction in Residual Field Around Indentation in Machined Glass Surfaces 28

5.2 Enhanced Strengths Observed in Machined Specimens with Indentation Flaws 32

Page

5.3 The Evolution Characteristics of Indentation Crack under an Applied Stress. 33

5.4 Evaluation of Residual Stress Parameter of Indentation Crack. 37

5.5 The Reduced Crack Size of Indentation on the Machined Surfaces. 38

5.6 Fatigue Characteristics of Machined Glass with Controlled Indentation Flaws 41

6. Conclusions. 43

ACKNOWLEDGMENTS 45

References. 46

Figure Captions 52

CHARACTERIZATION OF MACHINING DAMAGE IN GLASS

Hsiao-chu Tsai
(Ph. D. Thesis)

Department of Materials Sciences and Mineral Engineering
Lawrence Berkeley Laboratory
University of California, Berkeley, CA 94720

ABSTRACT

The material removal during diamond grinding of soda-lime glass appeared to occur by symmetric brittle chipping, probably due to lateral cracks. Indentation cracks in machined surfaces tend to exhibit irregularities at lower indentation loads and chipping at higher loads. The cracks are consistently smaller in size on the machined than the as-received specimens and no effect of annealing is noticeable. The moderate enhancement of resistance to strength degradation by machining occurs also when residual stresses are not involved. Therefore, the existence of machining-induced compressive residual stresses is not substantiated for glass.

The identation-induced residual stresses are observed in as-received glass. However, negligible precursor crack growth is measured during strength test of machined glass. Furthermore, the strengths of machined glass remain unchanged upon annealing after indentation. Thus, the residual stress effect about indentation is minimal in machined glass. A coherent explanation of these observations has been proposed.

1. INTRODUCTION

The shaping and surface finishing of brittle solids invariably involves grinding or abrading with sharp and hard grits. This process has several effects upon the strength of brittle solids, such as ceramics. The penetration and indentation of abrasive particles create a rough surface with machining-induced cracks as well as a thin plastic layer underneath the surface (fig. 1a). The penetration is surrounded by a plastic zone which accommodates the volume of penetration. Thus, an outward-acting pressure develops in the plastic layer, which creates compression in the zone and tension at the boundary of the plastic zone and beneath the zone (fig.1b). The residual tension beneath protuberances in the plastic layer may nucleate cracks which degrade the mechanical strength, whereas the residually compressed plastic layer inhibits surface crack formation from post-machining surface contact events (i.e. from project impacts, sliding contacts etc.). The competing influences of the strength-degrading dominant flaws and the compressive plastic player in a machined surface had been demonstrated in Si_3N_4,[1] Al_2O_3,[2] and glass-ceramics.[3]

It is known that the extent and magnitude of machining flaws and plastic layers is dictated by the mechanical properties and the material-removal mechanism. For instance, Kirchner and Isaacson[4] have observed the effect of residual stresses in strength measurements from single-point machining damage in steatite and Si_3N_4, but not in glass and silicon carbide.

The deformation and fracture created by individual particle contacts during machining resemble the damage associated with the single indentation by a sharp indenter which is dominated by the residual stress. Most previous studies[1,2,3] have provided evidence of this resemblance. However, the different material removal characteristics of various materials are expected to result in differences in the micromechanics of crack formation and propagation.

It is well known that the strength of a brittle solid depends to a large extent upon the surface flaws and the mechanical state of the surface. Therefore, the dominant flaws and associated residual stresses in the machined surface determine the structural performance of ceramic components. The intent of the present study is to examine post-machining strength characteristics of soda-lime glass, in order to expand and deepen understanding of the effect of machining on strength characteristics. The selection of soda-lime glass as a model brittle material in the present study avoids the interference of microstructure and anisotropy on mechanical behavior.

2. BACKGROUND

2.1 Material removal in ceramic machining

Machining of ceramic parts is generally performed by grinding. Grinding is a complex process involving the interaction of numerous abrasive particles embedded in the grinding wheel with the workpiece material. Unlike ductile materials, for which material removal is known to occur by a shearing process,[5] ceramic removal by grinding

is believed to occur by a mechanism of microfracturing with or without concurrent plastic flow, depending on the load and material properties.

By observing single-point scratches in glasses and alumina, Swain concluded[6] that at low loads ($P<0.05N$) no cracking was visible and the rate of plastically-controlled material removal was low. At intermediate loads ($0.1N<P<5N$) well defined median and lateral cracks occur. At higher loads ($P>5N$) the plastically deformed track appears to shatter and material is removed by microcracking or chipping which corresponds to typical "abrasion" operations on brittle solids. The latter case was characterized by rapid material removal and invariably leaves a rough surface. Similar phenomena were also observed during scratching of manganese zinc ferrite at different loads.[7] The fluctuations in the tangential force observed during scratching experiments on ceramics were related to the occurrence of chipping and cracking.[8] Because a moving indenter always encounters defects in the material that can develop into a crack, chipping or cracking will certainly happen somewhere along the scratch if the stresses around the indenter are large enough.

The threshold force for crack initiation in a moving elastic/plastic indentation fields was found related to the basic deformation/fracture parameters of the material (hardness and toughness)[9] as well as the distribution of pre-existing flaws with certain stress-concentration factors beneath the surface.[7,8] Therefore, the mechanism of material removal is expected to vary with workpiece material characteristics. Evidence of plastic deformation occurring in Al_2O_3

during abrasion was provided by transmission electron microscopy,[10] X-ray diffraction,[11] scanning electron microscopy[12] and electron diffraction.[13] The extent of the contribution of plastic flow to the material removal also depends upon the grinding conditions, such as the kind of abrasive particle used. For instance, the glass removal process by grinding at small depths of cut (<0.25μm) was found to occur by chipping when a silicon carbide grinding wheel was used, while a ploughing process apparently occurred when using an alumina grinding wheel.[14] Since plastic deformation occurs during indentation and abrasion by sharp indenters (which will be discussed further in later sections), purely brittle chipping rarely occurs. By comparing the measured specific energy (the energy required to grind away an unit volume of material) with the predicted values from proposed models, Veldkamp and Wassink[7] revealed that, in practice, the behavior of most brittle materials during grinding is best described by a behavior intermediate between ploughing (plastic cutting) and ploughing plus brittle cracking.

The cone cracks or Hertzian fracture created by fully elastic indentation rarely cause material removal. However, lateral cracking developed during unloading of elastic/plastic indentation can lead to material removal. A lateral fracture model has been proposed by Evans for material removal of brittle materials during abrasion.[15] The analysis of fracture-dominated wear processes in brittle solids based on this model indicated a reasonably good correlation with available experimental data.[16]

Lateral cracking occurs above a threshold force. The fracture threshold signifies a change in material-removal mechanism and a concomitant order-of-magnitude increment in removal rate. Below the threshold an operative mechanism involving plastic cutting may occur. The exact mechanism of this grooving or ploughing process is at present uncertain. Nevertheless, lateral cracking is expected to play a major rate in commercial machining of brittle materials.

2.2 Stress Field and Microfracture Beneath an Indenter under Normal and Horizontal Forces

(a) Elastic Stress Field and Microfracture Geometry.

As an extension of a previous study on the stresses beneath an axially symmetric sharp indenter,[17] the elastic field induced by both normal and horizontal point loads was studied by Swain.[18] It is noted that σ_{11} is tensile and σ_{33}--compressive everywhere, while the hoop stress σ_{22} is tensile beneath the indenter and compressive outside a conical region. The relative magnitudes of principal stresses indicate that $\sigma_{11} > \sigma_{22} > \sigma_{33}$ and $\sigma_{11} >> \sigma_{33}$.

In a brittle solid the tensile stress is the primary component responsible for the operation of fracture processes. A crack, once initiated when a critical load was reached, will tend to propagate along trajectories of principal normal stresses, thereby maintaining orthogonality to a major tensile component. This was demonstrated by the evolution of a Hertzian crack under a blunt indenter. A crack initiated directly below the point of a sliding sharp indenter will tend to grow downward along the axial σ_{33} trajectory and expand in

alignment with the track but in the opposite direction to sliding.[6] Thus, in the case of a sliding sharp indenter, only one median crack aligned along the track survives and produces a continuous "trailing" median vent beneath the scratching point.

Although it was observed in quasi-static indentation that penny cracks formed during loading continue to grow toward the specimen surface as the indenter is withdrawn, the final half-penny crack maintains the same depth as the one attained at the end of loading. Hence the median crack depth can uniquely be determined by the stress field with aid of linear elastic fracture mechanics (LEFM).

(b) Elastic/Plastic Indentation

Because of a stress singularity at the point of contact, plastic flow typically occurs before cracking. Unlike the fully elastic contact of a blunt indentation, the indentation with plastic penetration is complicated by further developments in the crack pattern upon unloading. On unloading, the elastically deformed material surrounding the plastically deformed zone is constrained from returning to its original equilibrium position. The result of this incompatibility is a residual stress field which begins to dominate the field of the applied loading just prior to complete removal of the indenter. This residual field contains a tensile component large enough to generate an entirely new, laterally extending system of cracks.[17,19] Unlike the median cracks which is relatively well defined as shown in previous section, the lateral vents which originate from residual

stresses associated with the irreversible deformation zone are, unfortunately, less easily modelled.

Upon withdrawal of indenter, the irreversibly deformed zone acts as a center of contraction with respect to the surrounding elastic matrix. This is directly responsible for the formation of a residual field and lateral as well as radial cracking. The σ_{33} stress normal to the lateral vent becomes one of the dominant components of tension in the field and creates a lateral crack system. This plastic stress field has been modelled by using Hill's solution[20] of an expanding cavity under pressure in an infinite elastic/plastic matrix.* For instance, in a recent attempt, the plastic zone-related stress field, as modelled by Chiang et al.,[22] features the existence of a peak tension at the elastic/plastic boundary, a rapid transition into compression within the plastic zone, and a monotonic decrease in the tension at progressive distance into the elastic matrix. These characteristics suggest that lateral cracks would usually initiate in the vicinity of the elastic/plastic boundary and extend primarily into the elastic zone. This behavior appears consistent with the well-established observation that lateral cracks evolve at the boundary during load removal.

---

* From ref.21:
The tangential stress within the plastic zone in an infinite body at a distance r from the center is given for a perfectly plastic material by

$$(\sigma_\theta^p/\sigma_\gamma) = -2 \ln (r_p/r) + 1/3 \qquad \text{(i)}$$

where r_p is the plastic zone radius and σ_γ is the uniaxial yield stress; while the elastic stress is

$$(\sigma^e/\sigma_\gamma) = (r_p/r)^3/3 \qquad \text{(ii)}$$

The method of analysis by approximating the deformation zone to a hemispherical cavity appears to be adequate to the determination of the residual stress field. Because of the hemispherical symmetry of the plastic zone (regardless of indenter shape) and the stress-free nature of the indentation surface, the residual stresses within the elastic zone are relatively insensitive to the indenter geometry, for a specified plastic zone size. Fortunately, the ultimate dimensions of indentation fractures are dominated by the residual field[23,24] and thus the extent of an indentation fracture is related to the indentation volume, independent of the indenter shape.[22]

Whereas the critical formation load for radial cracking exhibits a significant dependence on the surface condition, the crack formation load for lateral fracture shows independence on surface condition. The implication is that unlike the radial cracks which originate from pre-existing surface flaws, lateral cracks form in the vicinity of the elastic/plastic boundary. This is the basis for quantifying the material removal by lateral fracture proposed by Lawn[25] and Evans et al.[16] as will be discussed in the next section 2.3.

For a sliding indenter the residual stresses are only symmetric in a plane perpendicular to the scratch direction. A model that is physically realistic and at the same time sustains the cavity analogy is that of a cylindrical cavity under pressure in an elastic half-space adjacent to the surface.[6] Strong support for this approach comes from photoelastic observations of subsurface stresses beneath a scratch on glass by a diamond indenter. In front of and beneath the

moving indenter a region of compressive stresses occurs, whereas behind and at the sides of the indenter large tensile stresses occur.[6] Thus, the lateral cracks form continuously in the wake of the indenter from the plastically deformed zone and propagate along an angle outward from the median plane.[7] It was also observed[26] that lateral chipping about the machined groove did not occur until some time after the diamond point had left the surface, consistent with the residual-stress origin of lateral cracking.

2.3 Lateral Fracture Model of Material Removal

The tangential out-of-plane tensile "hoop" stress σ_{22} at surface developed by plastic penetration, and enhanced by friction between a sliding indenter and the surface, accounts for radial cracking. The in-plane σ_{11} at the elastic/plastic boundaries could account for the formation and preliminary propagation of lateral cracks in the subsurface, adjacent to the impression. However, the subsequent extension of these cracks towards the surface is not explained since the tension trajectories ultimately orient away from the surface. The probable reasons are suggested to be: (1) the stress field changes due to the propagation of a crack in the vicinity of surface, such that the crack trajectory should not be expected to resemble the prior tensile stress trajectory. (2) The resemblance of each of the lateral crack trajectories to the principal shear stress trajectories suggests the possibility of mixed mode fracture.

Lawn[25] and Evans et al.[27] proposed models of material removal by fracture when lateral cracks intersect each other or propagate to the surface. Evans and Wilshaw[27] predict the upper limit for materia removal rate (volume per unit area per unit sliding distance)

$$V = N\bar{P}^{5/4}/K_c^{3/4}\ H^{1/2} \tag{2.1}$$

where $\bar{P}$ is the mean normal load per particle, N - number of particles that contact surface per unit area, K_c - fracture toughness, H - hardness. The available data are consistent with the predicted dependence on the load, the hardness and the fracture toughness.

In a similar approach, Evans and Marshall[16] derived another equation for material removal by treating the lateral crack as a thin cantilever opened by a residual force exerted by the plastic zone. The prediction of force exponent of 5/8 for the lateral crack extension appeared consistent with the measurements conducted on MgZn ferrite. The volume removed by fracture mechanism is given by

$$V = \alpha N P_n^{9/8}(E/H)^{4/5}/K_c^{1/2}H^{5/8} \tag{2.2}$$

where α is a material-independent constant and P_n is the peak load during particle penetration.

The present predictions on both the material removal rate and the grinding forces with the material parameters (K_c and H) of brittle solids indicate a reasonably good correlation with available experimental data.[16] The correlation substantiates the strong importance of both the fracture toughness and the hardness upon the material removal rate. The success of this simple lateral crack model suggested

that most of the proposed complexities do not impose additional material-dependent influences upon the material removal process.

2.4 Indentation Plasticity in Brittle Surfaces

The analysis of indentation stress field in the previous sections is applied to the "normal" brittle solids, as typified by most crystalline solids and silicate glasses with a substantial component of network modifiers in their structure, such as soda-lime glass. However, abnormal mechanical properties were observed in indentation of silica-rich glasses due to the densification that occurs beneath the indenter. The explanation of these anomalous behaviors rests with the compaction of more "open" silica network, in particular with the relative movements of atoms in the Si-O-Si linkages between the network tetrahedra; modifying ions are regarded as restricting these movements. In case of "normal" brittle solids, the stress field and microfracture of indentation are dominated by the residual stress field which arises from the constrained plastic deformation in accommodating the indentation volume. While densification of material occurs beneath the indentation, less accommodation was needed for the impression. It thus results in a reduced residual stress field around the irreversibly deformed zone, as observed by birefringence.[28] Consequently, anomalous glasses exhibit different indentation crack pattern from that of normal glasses.

The contact field of indentation is primarily one of compression and shear, thereby allowing an irreversible deformation to occur in brittle materials, regardless of its brittleness. Whereas in fused

silica densification was observed beneath indenter, devoid of any shear line rosettes that occur in soda-lime glass;[29] the normal glasses deform largely by a shear-dominated flow process.[28] The slip appears as shear faults with slip occurring in atomically sharp boundaries in normal glasses.[30] The role of modifying ions in the structure is then seen as one of providing "easy-slip" paths through an otherwise rigid, strongly covalent network (inhomogeneous shear).[31]

It was noted for normal glasses there is a departure from ideal plastic behavior which requires the spiral flow lines should meet at 90°; however, because of densification, these flow lines meet at about 110° in the bulk and intersect the specimen surface at 50° instead of 45°.[30] Thus, the indentation in normal glasses combines the effects of plastic flow and densification.[32]

The depth of deformed zone, a zone of shear flow and fracture, was shown to be proportional to the square root of vertical indenter load, i.e. $Z_0 = \beta(P/\alpha\pi H)^{1/2}$, where β and α are dimensionless geometrical factors. Computations indicated that in case of scratching and grinding, the horizontal load component had very little effect on the depth of deformed zone Z_0.

2.5 Crack Initiation in Elastic/plastic Indentation

Of two major sequences in indentation cracking, propagation is relatively well understood, for it is in a stage of growth that the fracture mechanics treatment of a "well-developed" crack is most applicable. However, in the initiation stage the dependence of crack

nucleation and formation processes on a multiplicity of structural and specimen history factors that tend to introduce complications, among them, for instance, the issue of flaw statistics.

During loading of an indenter, small flaws which always exist in the surface of brittle solids cause shallow surface Hertzian-like ring cracks to form just outside the area of contact. When the load is increased, these ring cracks propagate into fully developed Hertzian cone cracks in anomalous glasses, whereas in normal glasses they become absorbed within the area of contact and propagate along subsurface shear-stress trajectories.[33] When the load is further increased, median cracks may form in fused silica but usually initiate at the surface, whereas in normal glasses median cracks initiate subsurface in the vicinity of the elastic/plastic boundary where a peak tension was predicted.[22] The latter is the case normally observed in the loading half-cycle of elastic/plastic indentation and attracting most interest because in all other cases cracks mostly initiate from preexisting surface flaws and thus provoke nothing but a classic problem of fracture mechanics.

Based upon the empirical evidence of subsurface crack source of elastic/plastic indentation in normal glasses, Lawn and Evans proposed a model[9] to predict critical conditions for the initiation of the subsurface cracks in elastic/plastic indentation. Their model implies the existence of subsurface flaws of critical dimensions in the vicinity of the elastic/plastic boundary where the tensile stresses are highest. The stress field was approximated by a linear profile and

evaluated by using Hill's solution for a pressurized spherical cavity. In this very simplified way, they have shown that the minimum load to propagate the critical flaws is

$$P_c = (54.47\alpha/\eta^2\theta^4)(K_c/H)^3 K_{Ic} \tag{2.3}$$

The size of the corresponding critical size is given by

$$C_{min} = (1.767/\theta^2)(K_c/H)^2 \tag{2.4}$$

where θ, η and α are dimensionless factors related, respectively, to the peak stress at the elastic/plastic boundary beneath the indenter, the spacial extent of the tensile field, and the indenter geometry.

The importance of the deformation to the nucleation of various cracks around the indentation is highlighted by the observation of Vickers indentation in single crystals of LiF[34]. Shear cracks under indentations are formed by the interaction of dislocations on intersecting (110) 90° and (101) 45° planes. The cracks under Vickers indentation thus nucleate essentially from the interaction of dislocations on two intersecting slip planes or from one slip plane blocking dislocations on another slip plane. This provides a mechanism for producing flaws in crystalline solids during the deformation process. The critical loads P_c and critical flaw sizes predicted by this theory are lower than those of Lawn-Evans model, although two theories predict the same relationship: $P_c \sim K_c^4/H^3$.

Similarly, the nucleation of the subsurface median cracks in soda-lime glass, as observed by Hagan and Swain,[35] is a result of the interaction of the two limiting flow lines (inhomogeneous shear lines).

Concerning the lateral cracks which evolve upon unloading, these authors noted[35] that unlike crystalline solids where deformation is by dislocation motion, shear deformation in glasses in the absence of any long range order is non-constructive and the overstraining of atomic bonds leads to bond breakage and degeneration into shear cracks. These shear cracks probably initiate a local weaknesses in the highly strained region beneath the indenter and under certain favorable conditions propagate to become lateral cracks during unloading (compressive stresses prevail whilst under load).

In summary, the ability to form any kind of the indentation cracks (median, radial and lateral) is related to the formation of shear crack about the area of contact.[33] The resistance of a material to shear is generally a function of the interatomic bonding strength. It was found that with increasing silica content of soda-lime glass, the stress to nucleate shear crack increase.[36] Also the densification of glasses is enhanced by the increasing content of glass former (silica). Consequently, two mechanisms appear to oppose crack nucleation and growth in glasses with increasing concentration of glass former; i.e increasing difficulty in forming shear cracks and decreasing magnitude of the residual stress about the indentation impression.[33]

2.6 Residual-stress Effects in Strength Characteristics

As discussed in previous sections, in an elastic/plastic indentation the stress field is composed of elastic and residual components. The residual field arises from mismatch tractions exerted on the sur-

rounding matrix by irreversibly deformed material. This component persists as the indenter is removed. Therefore, residual stresses are responsible for the formation and growth of lateral and radial cracks which occur during the unloading half-cycle. The propagation of radial cracks and, in particular, lateral cracks tend to partially relieve the residual stresses around the indentation. However, residual opening forces still remain around indentation cracks. Th existence of residual crack mouth-opening forces was confirmed by optical birefringence observation.[37] When specimens with controlled flaws by sharp indenter are broken in strength testing, the critical stress intensity factor, K_c, calculated from measurements in the tests was consistently lower than those determined by more conventional methods, typically by 30%.[38] Moreover, it was found that when the surface of Si_3N_4 specimens with indentation impression was either ground away or annealed, the new K_c values determined in strength testing were in good agreement with double torsion data.[38] Such evidence is another indication of a residual opening force on the indentation cracks.

Since the indentation cracks evolve predominantly during the unloading half-cycle, the residual field has an eminent effect on the formation and growth of indentation cracks. Moreover, its effects on post-indentation strength characteristics are extremely important to the performance of brittle materials.[23,37,39,40] The basic approach in formulation of strength theory is to subdivide indentation driving force for the fracture into well-defined components and then using the

additive properties of stress intensity factors to derive the fracture mechanics relationships which govern the crack growth.

The characteristic crack dimension c° corresponding to an indentation load P is given by an equilibrium equation

$$K = \chi_e P/C^{\circ 3/2} + \chi_r{}^\circ P^*/C^{\circ 3/2} = K_c \tag{2.5}$$

where P* is the peak contact load and the dimensionless constant consists of components χ_e due to ideally elastic point loading P and $\chi_r{}^\circ$ due to elastic/plastic mismatch stresses about the deformation zone. The $\chi_r{}^\circ$ persists after removal of indenter, so the fracture mechanics relation governing crack growth in an applied tension σ_a becomes

$$K = \chi_r{}^\circ P/C^{3/2} + \sigma_a(\pi\Omega C)^{1/2} = K_c \tag{2.6}$$

where Ω is another dimensionless constant. An applied stress-crack size relation is by simple transformation:

$$\sigma_a = [K_c/(\pi\Omega C)^{1/2}](1-\chi_r{}^\circ P/K_c C^{3/2}) \tag{2.7}$$

with a maximum at

$$\sigma_m = 3K_c/4(\pi\Omega C_m)^{1/2} \tag{2.8}$$

$$c_m = (4\chi_r{}^\circ P/K_c)^{2/3} \tag{2.9}$$

by setting $d\sigma_a/dC = 0$. Hence, the residual stress term $\chi_r{}^\circ P/C^{3/2}$, by virtue of its inverse dependence on C, exerts a stabilizing influence on the crack growth. If $C^\circ < C_m$, the flaw grows stably with increasing σ_a until $\sigma_a = \sigma_m$, then give the instability stress

$$\sigma_m = \sigma_f{}^\circ = 3K_c^{4/3}/4^{4/3}(\pi\Omega)^{1/2}\chi_r{}^{\circ 1/3}P^{1/3}. \tag{2.10}$$

Thus the strength, expressed in σ_m, can be increased if the residual stress intensity χ_r were to be reduced by removing the source of the

residual stresses, i.e. the deformation zone: progressive surface finishing,[38] annealing[40,41] and acid etching[42] are examples of such treatments. Typically, specimens with controlled indentation flaws yield strength data which tend to lie some 30% below that determined by conventional fracture testing techniques.

Other than the strength degradation effect, the residual opening force on indentation cracks has its effect in several aspects of strength characteristics of brittle materials:

(a) The residual-stress component in the crack driving force imposes an energy barrier to failure so that the as-indented specimens experience a relatively large extent of subcritical crack growth in strength testing. If no slow crack growth occurs between indentation event and strength test ($\chi_r = \chi_r^\circ$), the pertinent starting crack dimension is C° corresponding to $P = 0$ in Eq. (2.5), i.e.

$$C^\circ = (\chi_r^\circ P^*/K_c)^{2/3} \tag{2.11}$$

comparison with Eq. (2.9) gives $C^\circ/C_m = 1/4^{2/3}$ or $C_m/C^\circ = 2.52$. Such precursor stable crack growth was observed experimentally. Specimens annealed after contact exhibit negligible subcritical crack growth prior to failure and thus confirm the existence of residual stresses.[40]

(b) Another effect of residual stress is a prospective acceleration of slow-crack-growth effects in nonequilibrium situations. Such effects would be expected to enter strongly into stress/life-time prediction. The lifetime at any specified level of stress is governed

by the velocity of the subcritical growth, which, in turn, may take the form[39]

$$v = v_0 \exp[B(K/K_c)] \qquad (K<K_c) \qquad (2.12)$$

where v_0 and B are constants. Substituting Eq. (2.6) and (2.9) then gives

$$v' = v_0 \exp[B(C_m/C)^{3/2}/4]\exp[B\sigma(\pi\Omega C)^{1/2}/K_c] \qquad (K<K_c) \qquad (2.13)$$

Introducing the residual stress term, therefore, effectively increases the crack velocity by a factor of $\exp[B(C_m/C)^{3/2}/4]$. For example, at $C = C_m$, using B = 33 evaluated from the room temperature data for soda-lime glass in water, this factor has the value 3.8×10^3.[39] It is pertinent that v_0'/v_0 has its maximum value at $C = C^\circ$, i.e. in the initial stage of crack growth which assume a controlling influence in the lifetime calculations.

Test results[41] demonstrate clearly that residual contact stresses can have a significant detrimental effect on the properties of soda-lime glass.

(c) Time-dependent strength characteristic of soda-lime glass was recognized as a classic example of aging. For instance, a systematic strength increase of 40% could be realized by aging; in contrast, the post-indentation annealed specimens gave strengths in the same range after aging.[42] One of the interpretation of the age-strengthening effect is in terms of blunting of the crack tip. But recent experiments show the blunting theory is highly questionable.[42] It is thus believed that the strength increase is associated with relaxation of the residual crack-opening force due to slow growth of lateral cracks

during the aging process in soda-lime glass.[42] This residual-stress effect is expected to extend to most ceramics.[43,44] However, anomalous glasses which show a tendency to deform by densification rather than by shear-induced flow, and soft materials (with low H/E ratio), which tend to "pile-up" around the indenter rather than radially outward, would appear to be less susceptible to this effect.

In summary, the strength degradation of contact flaws and the age-strengthening effect are in fact the "two sides of one coin". Both of them are just the result of residual contact stresses caused by the elastic/plastic mismatch of indentation. To demonstrate the difference between the strength behavior for indentation flaws with and without residual stresses, simple calculation appears helpful. For a radial crack in size of C° under uniaxial tension, conventional strength theory gives the strength without residual stresses as

$$\sigma^\circ = K_c/(\pi\Omega C^\circ)^{1/2} \tag{2.14}$$

So that, in conjunction with known ratio $C_m/C^\circ = 2.52$, Eqs. (2.8) and (2.14) give the strength ratio

$$\sigma^\circ/\sigma_m = (4/3)(C_m/C^\circ)^{1/2} = 2.12 \tag{2.15}$$

Thus the presence of the residual field may theoretically reduce the strength by more than a factor of two, if no slow crack growth occurs between indentation and strength-test events. But in practice because of the post-indentation growth, a reduced strength degradation was observed.

3. EXPERIMENTAL

Four-point flexure tests were conducted on as-received and machined soda-lime silicate glass beams with cross section 10 by 3 or 5 by 3 mm. All specimens were annealed prior to machining or testing, as needed to relieve initial residual stresses. The surface machining of specimens was performed on a surface grinder* with a metal-bonded 150-grit diamond wheel (6" by 0.5"), operating at 3450 rpm, and using a commercial water-based coolant. The machining direction was, in all instances, normal to the long axis of the test specimens, as required to have the most severe cracks oriented nearly normal to the strain axis.[45,46] The incidence of edge failures was minimized by polishing the edges of each specimens with 600-grit SiC paper, into a bevelled morphology, after machining. The surface grinder was operated in a mode having both constant feed rate (0.07 ms^{-1}) and constant depth of cut, d, such that d could be used as a systematic grinding variable.

Some tests were conducted in the as-machined state. However, in most instances,one or two widely spaced Vickers indentations were placed within the uniformly stressed (innerspan) section of the bend-test specimens. All indentations were oriented such that one set of cracks was normal to the strain axis. The surface traces of the indentation cracks were measured before and after strength testing.

---

* K.O.Lee, Aberdeen, SD

Such measurements were facilitated by using a dye penetrant* to highlight the crack (fig. 2). Furthermore, since indentation cracks in soda-lime glass are subject to stress corrosion and extend slowly with time, after indentation even when immersed in oil, all crack size measurements were made at least 24 h after indentation when crack size became stable.[47]

Fracture tests were conducted by an Instron 1122 testing machine. Since brittle solids such as soda-lime glass have low compliance and undergo little, if any, inelastic deformation before failure, special care should be taken to minimize errors which may occur in bend test due to unequal moment, twisting, wedging stresses and pin-specimen friction. Therefore, a fixture design, described by Hoagland et al.,[48] with tiltable and free-to-roll pins was used in the bend test. The inner span of the fixture was 14.1 or 12.7 mm, and outer span: 45.1 or 25.4 mm. Strength tests were conducted at a constant strain rate of 10 $MPa \cdot s^{-1}$, in an oil environment, as required to minimize slow crack growth during the fracture test.[23]

After flexure the broken specimens were examined routinely to ensure that only those with failure originated from indentation site (or from machining flaws where failure from machining damage was being studied) were used in statistics.

In each group of specimens for strength tests (about 10 points per datum) usually two specimens were emplaced with two indentations

* DP40, Doublecheck penetrant, Sherwin, Ind., Los Angles, CA.

spaced 2 mm apart along the longer axis, for the purpose of measuring the precursor crack growth before failure.

In some cases, specimens were annealed, between 500 and 600°C, for 2 to 24 h, after machining, as required to relieve residual stresses induced during machining. Indentations were then emplaced into the annealed specimens, using the above procedures.

4. RESULTS

4.1 Crack Length

Measured trends in the indentation crack radius with load, obtained for as-received and machined specimens, are summarized in fig. 3. The results represent an average of at least 10-16 measurements over the two orthogonal radial traces for each condition. The indentation cracks are, on average, significantly smaller on the machined than the as-received specimens. The indentation crack radius, C_i, obtained on the as-received specimens vary with load P, as $C_i \sim P^{2/3}$, consistent with prior studies.[49] However, the indentation crack lengths on the machined surfaces exhibit considerably greater variability, as evident both from the cumulative distributions of normalized crack radii (fig. 4) and from the variable crack paths (fig. 5) in the machined surfaces. Furthermore, the crack length distributions are relatively insensitive to the depth of cut.

Annealing of machined specimens before indentation to relieve the residual stresses induced by machining caused no significant change in the indentation crack radii (fig. 6). Both the crack length average

and the standard deviation remain essentially invariant, with the average indentation crack radii always being appreciably smaller than those induced on as-received surfaces (fig. 6).

After strength testing, those indentation cracks normal to the strain axis that did not cause the failure were observed to increase in radius. Typical trends in the normalized crack length increment, $\Delta C/C_i$, are plotted in fig. 7. The relative crack growth on as-machined surfaces is consistently small, and essentially insensitive both to the depth of cut and the indentation load, such that $\Delta C/C_i$ = 0.08 ± 0.05. However, the as-received materials exhibited substantially more variable behavior, such that $\Delta C/C_i$ ranged between 0.3 and 0.8 for small indentation loads (~10N) but reduced to only ~0.1 at higher loads (80N) Post annealing also affected the precursor growth of the indented, as-received specimens (fig. 8). Notably, annealing above ~520°C for 24h or above ~580°C for 2h completely eliminated the precursor growth, consistent with relief of the indentation induced residual stresses.

4.2 Strengths

The strengths of as-received and machined specimens (10 specimens per datum) are plotted as a function of indentation load in fig. 9. The results are insensitive to the depth of cut. The as-received specimens exhibited a monotonic decrease in strength, S, with increase in load, P, such that the theoretically predicted proportionality,[40] $S \sim P^{-1/3}$, approximately obtains. The strength characteristics of the machined specimens are considerably more complex. When the

strengths are less than the median strength measured on as-received, indented specimens, fractographic observations reveal that fracture generally initiates from machining damage and not from the indentation crack. Conversely, when fracture initiates from the indentation crack, the strength typically exceeds the median strength measured on as-received specimens, at the same indentation load. The transition from failure dominated by machining damage to failure from indentation cracks occurs at an indentation load of ~15N, corresponding with a strength of ~55 MPa and a crack radius of ~100μm. Hence, the present studies indeed confirm that machining can enhance the contact degradation resistance of a material, albeit that the effect only obtains above a damage threshold (dictated by the severity of the machining damage).

The strength of specimens subject to annealing treatments, after machining and indentation, are essentially the same as those exhibited by the machined specimens, at least when the strength is dominated by machining flaws (fig. 10). Conversely, the strengths of the indented, as-received specimens increase consistently upon annealing, by ~1.2-1.3 (fig. 11).

4.3 Morphological Studies

Various morphological consequences of machining and indentation have also been observed using scanning electron and optical microscopy. A typical machined soda-lime glass surface ground by a diamond wheel, as depicted in fig. 12a, reveals that material removal appears to occur by symmetric brittle chipping. There is little evidence of a

plastic layer, manifest in other materials as plastic grooves, and no striations were observed along the grinding direction (fig. 13). The morphological similarity between machined surface at higher magnification (fig. 12a) and the chipped regions induced by the lateral cracking of indentation (fig. 12b) implies that the material removal during glass grinding by a diamond wheel appears to occur essentially by a fragmentation process, probably due to lateral cracking.

The depth of cut in grinding appears to have no systematical effect on the morphology of machined surfaces (fig. 13), indicating the material removal mechanism characterized in the previous paragraph is applicable to various machining conditions.

Cross sections (fig. 14a) indicate the irregularity of the machined surfaces. Furthermore, surface undulations are enhanced by etching in HF prior to sectioning (fig. 14b), indicating the presence either of localized residual stress or of subsurface cracks (fig.15). In contrast to the etched machined surface (fig. 16b), the polishing effect of etching on as-received surface (fig.16a) on the same specimen is obvious.

Regular crack pattern can be obtained in machined surface at higher indentation loads (fig. 17b). However at lower indentation loads, crack patterns in machined surfaces exhibit substantial irregularities (fig. 18 and 19b) and non-planarity (fig. 5) compared with the normal crack in as-received surface (fig. 19a), variability in fracture path and crack length is indicative of either localized residual stresses, or local variations in the near-surface crack propagation resistance.

As revealed in SEM micrographs of fracture surface, a straight edge is normally obtained on the tension side of the as-received specimen (fig. 20a), whereas machined surfaces always exhibit irregular edges (fig. 20b). The irregularity is not only related to the undulations of machined surface (fig. 21a), but also involved the presence of numerous spalls at the edge (fig. 21b), indicating that extensive deflection by machining flaws occurs during the propagation of the dominant crack. This results in an irregular subsurface (fig. 22a) which differs from the otherwise flat and smooth fracture surface characteristic of soda-lime glass. The irregularity of the subsurface region can be aggravated by the occurrence of spalling at the edge, as illustrated in fig. 22b. The extent of roughness created at the fracture edge is then enhanced to about 15-50 μm, which is significantly larger than the peak-to-trough heights of the original machined surface prior to fracture (~5 μm), as observed by cross-sectioning (fig. 14a). The depth of machining damage is thus 3-10 times greater than the roughness of the machined surface. The former can also be characterized by chemical etching, as shown in fig. 15, in which grooves up to 25~35 μm in depth were observed.

Finally it is noted that, at high load, indentations placed on machined surfaces exhibit considerable susceptibility to chipping by lateral crack propagation (fig. 23). The lateral cracks have also been observed to extend with time and during the strength test (fig. 24), resulting in time dependent chip formation and a concomittant change in the local residual stresses. This reflects the relatively

sluggish development of the lateral cracks (with respect to the radials) as observed earlier.[43]

5. DISCUSSION

Since the grinding process might be envisaged as an accumulation of a vast number of indentations, a continuous thin plastic layer is presumably created by the penetration of the machining particles. This plastic layer with associated residual stress field in brittle surfaces plays an important role in the interpretation of the present experimental results of strength characteristics and crack lengths.

The residual tension beneath protuberances in the plastic layer may nucleate cracks (fig. 1) which degrade the material strength, as dictated by indentation fracture mechanics. The depth of these cracks or vents is estimated to be several times larger than the roughness of machined surface, as characterized by HF etching as well as SEM examination of the fracture surface. However, the presence of residual stresses is not readily perceivable and some indirect means are needed to characterize the residual stress field.

5.1 The Reduction in Residual Field around Indentation in Machined Glass Surfaces

It is well known that the flaws induced by indentation or abrasion are subject to a persisting crack mouth-opening force and thus leads to reduction in strength. This residual tension is known to arise from the constrained plastic/elastic deformation in the penetration of indenter or abrasive particles. The intensity of this

residual stress as characterized by an elastic/plastic parameter χ_r in Eq. 2.5, can be reduced either by annealing which can lead to total elimination of residual stresses (if temperature and time are adequate) and then restore the equilibrium failure stress,as predicted by Griffith theory, or by the relaxation of the elastic constraint about the plastic zone due to the incidence of lateral cracking and subcritical growth.[44] The latter effect can be perceived by concerning the integrity of the elastic matrix is impaired by the incidence of lateral cracks and buckling of the material between the lateral crack and the surface tends to relax the elastic/plastic mismatch at the deformation zone boundary (fig. 25a).

Both the lowering of failure stress and the presence of precursor stable growth during strength tests on specimens with controlled indentation flaws, was caused by the residual crack-opening force. The relaxation of this residual tension should thus result in higher strength S and smaller precursor crack growth, $(C_m-C_i)/C_i$. The abnormally high value of $SP^{1/3}$ of as-received specimens at higher indentation load (fig. 26) and decreasing value of $(C_m-C_i)/C_i$ of as-received specimens with increasing P (fig. 7) provide the evidence of reduction in residual tension by the relaxation effect of lateral cracking at higher indentation loads. The critical compressive force to generate buckling is known to be:[50]

$$P_{cr} = \frac{\pi^2 EI}{l^2} \tag{5.1}$$

where I is the smaller principal moment of inertia of the cross sec-

tion. Thus, the higher the indentation load, the larger length of lateral crack l, then the smaller force is needed to start buckling . This is the reason why the values of $SP^{1/3}$ at highest load (P = 78.5N in fig. 26) are appreciably larger than the $SP^{1/3}$ values at lower loads which demonstrate constancy over a certain range of indentation load. However, this is not the case for the trend of $SP^{1/3}$ measured in machined specimens that are invariably higher than the mean $SP^{1/3}$ of as-received specimens, represented by fitted lines in fig. 26 (computed over all specimens except the one at highest indentation load). This difference in behavior between as-received and machined specimens certainly relates to the difference in the residual stress field about indentation which has, as indicated earlier, important implications in the determination of strength characteristics.

The presence of surface roughness and of a subsurface plastic layer are the two factors which distinguish machined surfaces from pristine surfaces, with respect to strength characteristics. With a controlled indentation flaw induced in machined surface as shown in fig. 25b, the moment of inertia pertinent to buckling must be significantly smaller than that in as-received surface (fig. 25a) because of $I \sim h^3(h'^3)$ and $h' < h$, due to the roughness of machined surface. According to Eq. (5.1), a smaller I leads to a smaller critical load, thus an enhanced buckling by lateral cracking is expected to occur and reduce the constraint on elastic/plastic deformation in machined surfaces to a greater extent. As a consequence, the indentation crack in machined surface should experience an appreciably reduced residual

field. This hypothesis is found to be consistent with all observations derived from a comparison of the results for machined and as-received specimens.

(a) Because of irreversible nature of aging process, the larger the slow crack growth in the post-indentation period, the less the strength increase that can be attained upon annealing. It is noted that the presence of the residual field typically reduces the as-indented strength by 30-40%.[40,51] A strength reduction of about 15% is, however, observed for as-received specimens in this study. The existence of residual stresses in these specimens is demonstrated by the strength increase upon annealing, although less than the typical value expected when no stress corrosion occurs. This is due to the relaxation of residual stresses by lateral cracking which occurs during post-indentation slow crack growth.[42] An even smaller strength increase upon annealing is attained in machined specimens which is equivalent to a strength reduction of 3.8-8.6% due to residual stresses (fig. 10). Comparing with the strength reduction of as-received specimens under similar stress corrosion conditions, the smaller strength reduction of machined specimens reflects a reduced residual field, consistent with the previous hypothesis.

(b) Another consequence of reduced residual tension at the indentation crack in machined surfaces is the minimal precursor crack growth observed in strength test, i.e. the measured $(C_m-C_i)/C_i<0.1$, in contrast to 0.2-0.6 measured in as-received specimens (fig. 7). The latter values are already less than the equilibrium value of $(C_m^\circ-C^\circ)/C^\circ=$

1.52, indicating once again the reduction in residual stress intensity due to slow crack growth in both cases.

The presence of indentation-induced residual tension in as-received specimens that served as the driving force for precursor growth can be verified by the elimination of precursor growth upon annealing (fig. 8). However, the minimal presence of a residual field around the indentation in machined surface has changed the strength characteristics such that the applied stress vs indentation-induced crack size relation, Eq. (2.7) is no longer valid. This is confirmed by the correlation between strength, flaw size and toughness, based solely on the unstable branch of Eq. (2.7), i.e. the standard fracture mechanics relation for ideal full penny crack, $S=\sigma_f'=\sqrt{\pi}K_c/2\sqrt{C_i}$, using a value of K_c (0.75 MPa m) typical of soda-lime glass (fig. 27).

5.2 Enhanced Strengths Observed in Machined Specimens with Indentation Flaws

The strengths obtained for machined specimens are about 10% greater than that for as-received specimens with ostensibly identical indentations (fig. 9). This enhancement in strength is much less than that observed in Si_3N_4,[1] and glass-ceramics.[52] The latter is due to the substantial level of residual compressive stress introduced by machining damage (by a 400 grit diamond wheel).[51,52] The closure forces then act on the surface flaws, and any subsequent tensile loading must first negate these forces before becoming effective in driving the system toward failure. Because of the existence of energy barrier in the failure test of as-indented specimens, the initial crack size

C_i no longer plays a part in the strength determination. The strength increase is presumably a result of the closure effect of the compressive stress on the indentation crack during the strength test. If this is the case, the strengthening effect would be negated by an appropriate annealing treatment after machining but prior to indentation. However, no such change in strengths is observed with machined specimens (5 μm depth of cut) annealed prior to indentation: S=63.4±3.1 MPa (n=9) at P=9.8N and S=57.5±3 MPa (n=9) at P=19.6N, in comparing with the strengths of non-annealed machined specimens: 63.2±5.6 MPa (n=10) and 58.3±3.9 MPa (n=11) respectively--where n denotes number of measurements. Therefore, the proposed residual compressive stress effect is not substantiated by the current experimental data of annealing of machined glass specimens. The comparatively small enhancement in contact degradation resistance of glass by machining is thus related not to the residually compressed layer in machined surface, but to the reduction of residual crack-opening force due to enhanced lateral cracking in machined surfaces, as discussed in the last section.

5.3 The Evolution Characteristics of Indentation Crack under an Applied Stress

The evolution characteristics of indentation crack under an applied stress as expressed by plotting stress σ_a against crack length C is useful in quantifying the effect of indentation-induced residual stresses. There are two limiting cases of interest:

(1) The immediate post-indentation state designated by a superscript °, represents a theoretical case without stress corrosion. Since the newly created indentation crack is in equilibrium without slow growth, the residual stress intensity remains $\chi_r = \chi_r^\circ$ and the starting crack length is $C^\circ = (\chi_r^\circ P/K_c)^{2/3}$ due to Eq. (2.6) and $\sigma_a = 0$. On applying the tensile loading in the strength test the crack grows stably to a critical size $C_m^\circ = 4^{2/3}C^\circ$, and then grows spontaneously to failure, as expressed by Eq. 2.7. Using data for P = 49N: C° = 196 μm, C_m° = 491 μm and σ_f° = 30 MPa,[42] the failure path in this limiting case is represented by the lower dashed line in fig. 28.

(2) The annealed state, designated by a superscript A, is other extremity in crack evolution. The residual stresses are removed by annealing such that $\chi_r = \chi^A = 0$. Equation 2.7 now takes on an simple form: $\sigma_f^A = K_c/(\pi\Omega C)^{1/2}$ for P = 49N as represented by the upper dashed curve in fig. 28, which demonstrates completely different characteristics in crack evolution from those with a residual stress field.

In the present study, a post-indentation slow crack growth invariably takes place in soda-lime glass prior to the strength test. Since the post-indentation growth of lateral crack is effective in reducing the residual stress intensity χ_r, the crack evolution curves of these as-receives (χ_r) and machined specimens (χ_r') are, therefore, expected to lie between the two limiting curves, i.e., $0 < \chi_r' < \chi_r < \chi_r^\circ$. Two sets of strength and crack-length data at P = 49N measured in this work are selected and plotted in fig. 28: the solid and dotted lines to represent as-received and machined specimens,

respectively. These curves are distinguished from the limiting cases by the following characteristics:

(a) Because of post-indentation slow crack growth, the mean values of initial crack length measured in as-received and machined surfaces at P = 49N, C_i = 298 μm and C_i' = 280 μm respectively, are greater than the equilibrium length of indentation crack, $C^\circ = (\chi^\circ P/K_c)^{2/3}$ = 195μm.[42]

(b) The reduced residual field leads to lower precursor growth in the strength test. For as-received specimens, the average C_m measured from the indentation at P = 49N is 349 μm, i.e. C_m/C_i = 1.17 is much less than the equilibrium value, C_m°/C_i° = 2.52. For machined specimens the precursor growth is negligible (fig. 7) and thus an upper limit of growth (C_m'/C_i = 1.10) has to be adapted in constructing the dotted curve for machined specimens in fig. 27 to avoid overlapping the solid curve for as-received specimens.

(c) Another effect of the reduced residual field is the higher failure stresses σ_f = 40.4 and σ'_f = 47.2 MPa measured in as-re-ceived and machined specimens respectively, in comparing with the zero-age-time strength, σ°_f = 30.0 MPa corresponding to $\chi_r = \chi^\circ_r$ curve.[42] This aging phenomenon is now believed to be associated with the relaxation of the residual field by lateral cracking in slow growth and not related to the crack-tip blunting proposed earlier, as reviewed in (c) of section 2.6.

The failure stress σ_f or σ_m is correlated with χ_r, in Eq. 2.10, such that for as-received specimens

$$\frac{\chi_r^{1/3}}{\chi_r^{\circ 1/3}} = \frac{\sigma_f^{\circ}}{\sigma_f} = \frac{30}{40.4} \tag{5.2}$$

or

$$\chi_r = 0.41\ \chi_r^{\circ}\ . \tag{5.3}$$

Thus, because of post-indentation slow crack growth, the estimated residual opening force on indentation crack in as-received surface is reduced to less than one half of its immediate post-indent level. It is reported that through a prolonged exposure to a moist environment (immersion in water) the indentation flow at P = 49N undergoes slow growth until $C^{\infty} = 362\ \mu m$ (the superscript ∞ denotes the fully aged state, which is indicated by zero stable growth.[4]) The residual stress intensity in fully aged state is reduced to about a quarter of its optimum, immediate postcontact level, i.e. $\chi^{\infty} = 0.23\ \chi_r^{\circ}$.[42] This is about half of the residual force observed in as-received specimens (5.3). In other words, the application of oil immersion in the indentation and fracture tests reduce the stress corrosion and do maintain the residual field in as-received specimens.

(d) As the indentation crack in as-received surface grows from C° to C_i due to stress corrosion, the indentation-induced residual field is partially relieved. As a consequence, the strength increase upon annealing $(\sigma_f^A - \sigma_f)$, as shown in fig. 28, is much less than that obtained immediately after indentation. The minimal pres-

ence of residual stress in machined specimen leads to an even smaller strength increase upon annealing, as shown in fig. 28.

5.4 Evaluation of Residual Stress Parameter of Indentation Crack

Since the indentation cracks in soda-lime glass are subject to stress corrosion, the crack size measured prior to strength testing C_i is greater than C°, which is related to the indentation load P by an equilibrium equation, Eq. (2.11). Fortunately, a similar relation $C_i \sim P^{2/3}$ obtains for as-received specimens (fig. 3). An analogous equation is given in terms of fracture toughness, K_c

$$C_i = (\chi_r \, P/K_c)^{2/3} \tag{5.5}$$

with χ_r less than χ°_r in (2.11). Therefore, Eqs. (2.5) and (2.6) are applicable to the measured C_i of as-received specimens, and thus a similar expression can be written to depict the crack growth under an applied stress starting from C_i:

$$\sigma_a = \frac{K_c}{(\pi\Omega C_i)^{1/2}} \quad (1 - \chi_r \, P/K_c C_i^{2/3}) \tag{5.6}$$

When residual stresses are present, or $\chi_r > 0$ and $C_i < C_m$, failure can occur only if the crack is made to grow stably to C_m by increasing the stress to $\sigma_a = \sigma_m = \sigma_f$, then

$$\sigma_f = [27 \, K_c^4/256 \, \chi_r(\pi\Omega)^{3/2}P]^{1/3} \tag{5.7}$$

by setting $d\sigma_a/dC_i = 0$. Being a residual-stress-sensitive strength, this is, however, greater than the equilibrium strength σ°_f in Eq. (2.10) as $\chi_r < \chi^\circ_r$ due to stress corrosion.

Another case of interest corresponds to the limit, $X_r = 0$, i.e. indentations free of residual stress. This gives $C_m = 0$ in Eq. (2.9), so the function $\sigma_a(C)$, Eq. (2.7), has only an unstable branch, as shown in fig. 28 by the upper curve. This is pertinent to annealed specimens, which yield residual-stress-free strength,

$$\sigma_f^A = K_c/(\pi\Omega C_i)^{1/2}. \tag{5.8}$$

Thus, dividing (5.8) by (5.7)

$$\sigma_f^A/\sigma_f = \left(\frac{256\ X_r\ P}{27\ K_c}\right)^{1/3} \Big/ C_i^{1/2}\ . \tag{5.9}$$

By measuring the strength increase upon annealing (σ_f^A/σ_f) and the initial crack size C_i, the residual stress parameter X_r can then be determined. For instance, at an indentation load P = 9.8N, σ_f^A/σ_f = 1.18 (fig. 11) and C_i = 115 μm, then X_r = 0.016. This indentation coefficient obtains also from the intercept of the fitted lines in the fracture mechanics plots (P/P^* vs $C^{3/2}\ K_c/P^*$) for median and radial crack evaluation. The intercept for complete unloading of radial crack in soda-lime glass, in a dry N_2 environment, $X_r^R = 0.049$,[23] is appreciably higher than that obtained here.

5.5 <u>The Reduced Crack Size of Indentation on the Machined Surfaces</u>

Based upon substantial measurements of crack lengths at varied indentation loads P (figs. 3 and 4), the radial crack sizes are found about one third smaller on the machined specimens than the as-received specimens. The presence of residual compressive stresses in the machined surfaces has previously been proposed on basis either of stress measurements of polycrystalline Al_2O_3 by an x-ray diffraction tech-

nique,[2] or of strength testing with progressive removal of the machining damage.[3] It has also been suggested that the residually compressed plastic layer inhibits surface crack formation and propagation from post-machining surface contact events (i.e., from indentation, project impacts, sliding contacts etc).[1,2] However, because annealing of machined specimens before indentation caused no systematic change in the indentation crack lengths (fig. 6), the reduced crack size in machined surfaces cannot be interpreted in terms of the enhanced resistance to crack propagation caused by the residual compressive stresses. Therefore, only those unaffected by annealing treatment before indentation can be considered as the possible cause of reduction in indentation crack size on machined surfaces.

During loading half-cycle of sharp indentation, whereas the elastic driving force, being reversible, does enhance crack growth in the subsurface median orientation, it serves merely as a restraining force on the growth in the surface radial direction, because of the compressive nature of the elastic field of a indenter pertinent to these cracks during load application. This should be true for as-received or machined surfaces. The crack evolution sequence that the radial cracks develop primarily after load removal as observed experimentally in Vickers indentation[23,40] must therefore be applicable to all brittle surfaces. In other words, the measured surface radial lengths of indentation are formed mainly after the withdrawal of load, i.e., when residual stresses dominate. Furthermore, because of the existence of residual field due to the incompatibility at the elas-

tic/plastic interface, growth of radial cracks may persist long after completion of the indentation cycle if the environment is reactive. If a certain interval between indentation and subsequent measurement is set to allow the system to come to equilibrium with the environment, as in the present study, the measured dimensions of indentation crack C_i is the summation of radial crack growth in unloading plus the subsequent slow crack growth in the reactive environment. The lines fitted to $C_i(P)$ data measured with > 30 min. intervals[53] and with > 24 hr. intervals in the present work (fig. 3) both have slopes of about 2/3 on a logarithmic plot of C_i vs. P. The implication is that both stages of crack growth, the unloading half-cycle of indentation and the subsequent slow crack growth operate from the same driving force.

In an analogy of geometrical similarity which governs the relation between P and a (characteristic dimension of indentation impression),

$$P/a^2 = \alpha H = \text{constant} \tag{5.11}$$

an equation is given for the well-developed crack pattern of indentation in terms of the fracture toughness, K_c:

$$P/C_i^{3/2} = \beta\ K_c = \text{constant}. \tag{5.12}$$

Uncertainties in the fracture mechanics precludes a theoretical prediction of the numerical constant β. However, some empirical relations in the form of Eq. 5.12 were obtained for as-received and machined specimens (fig. 29). The constancy of $P/C_i^{3/2}$ for as-received glass specimens over various indentation loads is obvious,

whereas variance of $P/C_i^{3/2}$ prevails in machined surfaces. It is, however, noteworthy that all the $P/C^{3/2}$ values obtained on machined specimens are larger than the counterparts of as-received specimens. The systematic change in $P/C^{3/2}$ with machining, as shown in fig. 29, can only arise from the change in β. Physically, β can be regarded as a factor which relates the normal indentation force P to the effective center-loading force driving the penny-like cracks which is, in turn, related to the residual stress field. Therefore, the systematic change of β in fig. 29 can in fact be interpreted by the change in residual field caused by machining through a mechanism proposed earlier in section 5.1.

5.6 Fatigue Characteristics of Machined Glass with Controlled Indentation Flaws

The tendency for brittle glasses to exhibit limited lifetime under sustained loading is an essential element of structural design with brittle components. To follow the crack evaluation during the fatigue history and to avoid the problems of variability in strength testing, a convenient way is to introduce a dominant flaw by indentation. Then the stress intensity factor for dominant crack is the sum of residual-contact and applied-stress components, as expressed in Equation 2.6. For dynamic fatigue $\sigma_a = \dot{\sigma}_a t$, where $\dot{\sigma}_a$ = constant, combine with the velocity function,

$$V = V_o\left(\frac{K}{K_c}\right)^n \quad (K < K_c) \tag{5.13}$$

a differential equation for crack size obtains in terms of time:

$$\frac{\dot{C}}{V_o} = \left[\frac{\chi_r}{K_c} \frac{P}{C^{2/3}} + \frac{(\pi\Omega)^{1/2}}{K_c} \dot{\sigma}_a C^{1/2} t\right]^n . \tag{5.14}$$

This differential equation must be solved by an integration procedure for the time t_f to take the crack from its initial size (C'_o) to its final size (solution of Equation 2.6 at $K = K_c$, $dK/dC > 0$ branch) in the subcritical region. With t_f thus determined the strength $\sigma = \dot{\sigma}_a t_f$ follows.

In general, the integration of Equation 5.14 has to be carried out numerically. An important exception is in the Griffith limit, $\chi_r = 0$, whence the standard analytical solution

$$\sigma^\circ = (\lambda\sigma_a)^{1/(n+1)} \quad (\sigma^\circ < \sigma_i^\circ) \tag{5.15}$$

is obtained, where

$$\lambda = \left[\frac{2(n+1)}{(n-2)}\right]\left[\frac{K_c}{(\pi\Omega)^{1/2}}\right]^n / V_o C'^{\,n/2-1} . \tag{5.16}$$

Since the strength characteristics of machined glass is described closely by a standard fracture mechanics relation pertinent to Griffith flaws, $S = \sqrt{\pi}\, K_c/2\sqrt{C_i}$ (fig. 27), Equation 5.15 is considered as a proper solution for dynamics fatigue analysis of machined glass with controlled indentation flaws. Thus best fit strength vs. stress rate can be used to determine the crack velocity exponent n in Eq. 5.13 on the basis of conventional dynamic fatigue theory (i.e., on the assumption $\chi_r = 0$).

It is already known that residual contact stresses can have a significant detrimental effect on the fatigue properties of soda-lime glass and other ceramics which exhibit fatigue, particularly at lower stress rates.[41] This, therefore, suggests that in-service lifetimes for brittle components should not be predicted from fracture data without due consideration of flaw characteristics. For machined glass, as revealed in this study, an analytical solution, such as Eq. 5.15, can be applied because of the negligible presence of residual stresses about the indentation. However, for slightly-abraded glass was, a 17% reduction in inert strength due to the presence of residual stresses, was observed.[54]

6. CONCLUSIONS

(1) The material removal during diamond grinding of soda-lime glass appeared to occur by symmetric brittle chipping, probably due to lateral cracks.

(2) Indentation cracks in machined surfaces tend to exhibit irregularities and non-planarity, particularly at lower indentation loads. The machined surface layer apparently has different crack propagation characteristics than the bulk.

(3) Machined surfaces are susceptible to brittle chipping about the indentation due to lateral cracking, especially at higher indentation loads.

(4) Strengths of indented, as-received specimens increase upon annealing. Also, the precursor growth of indentation cracks in as-received specimens was substantial. Furthermore, the precursor crack growth can completely be eliminated by annealing. These are indications that residual contact stresses exist in as-received glass.

(5) Negligible precursor crack growth was observed during strength test of machined glass. Moreover, the strengths of machined glass remain unchanged upon annealing after indentation. Therefore, the indentation-induced residual stress effect is minimal in machined glass.

(6) When fracture initiates from the indentation crack, the strength of machined glass exceeds the median strength of as-received specimens, at the same indentation load. This occurs even when the machining-induced residual stresses are not involved (viz. annealing prior to indentation).

(7) The indentation cracks are smaller in size on the machined than the as-received specimens. No effect of post-machining annealing was observed. The reduced crack size has thereby been attributed to a reduced elastic constraint and an enhanced lateral cracking in machined surfaces which, in turn, relieves the residual opening-force on indentation cracks.

(8) The minimal influence of residual compressive stress on the mechanical behavior of machined glass is presumably a consequence of the predominant effect of lateral cracking, which causes extensive removal of the plastic layer during machining.

ACKNOWLEDGEMENTS

I thank all of the wonderful people who have enriched my experiences at Berkeley. I am particularly grateful to Professor Tony Evans for his invaluable guidance and support in this work. I would also like to thank Professors L. De Jonghe and Hari Dharan for critical reading and comments on the thesis. Special thanks to D. B. Marshall, R. Cannon, E. Case and C.-H. Hseuh for their help and friendship. Special thanks are extended to Mary Hammond, Gloria Pelatowski and June DeLaVergne for preparing the manuscript and figures.

Finally to my dear wife You-li and my family, who have supported me with their love through these years. my love and appreciation.

This work was supported in part by the Director, Office of Energy Research, Office of Basic Energy Sciences, Materials Sciences Division of the U. S. Department of Energy under Contract No. DE-AC03-76SF00098 and by the Office of Naval Research under Contract N00014-81-K-0362.

REFERENCES

1. D. B. Marshall, A. G. Evans, B. T. Khuri-Yakub, J. W. Tien and G. S. Kino, "The Nature of Machining Damage in Brittle Materials," Proc. R. Soc. London, A385, 461-475 (1982).
2. F. F. Lange, M. R. James and D. J. Green, "Determination of Residual Surface Stresses Caused by Grinding in Polycrystalline Al_2O_3," Am. Ceram. Soc., 66 (2), c16-17 (1983).
3. R. F. Cook, B. R. Lawn, T. P. Dabbs and P. Chantikul, "Effect of Machining Damage on the Strength of a Glass-Ceramic," J. Am. Ceram. Soc. 64 (9) c121-122 (1981).
4. H. P. Kirchner and E. D. Isaacson, "Contact Damage and Residual Stresses Induced During Single Point Grinding of Various Ceramics," pp. 57-70 in "Fracture Mechanics of Ceramics," v. 5, ed. R. C. Bratt, A. G. Evans, D. P. H. Hasselman, and F. F. Lange. Plenum Press, New York, 1983.
5. S. Malkin, "Grinding of Metals: Theory and Application," J. Appl. Metalworking, 3[2] 95-109 (1984).
6. M. V. Swain, "Microfracture about Scratches in Brittle Solids," Proc. R. Soc. Lond. A366, 575-597 (1979).
7. J. D. B. Veldkamp and R. J. Klein Wassink, "Grindability of Brittle Materials: A Theoretical and Experimental Investigation," Philips Res. Repts. 31, 153-189 (1976).
8. A. B. van Groenou, N. Maan and J. D. B. Veldkamp, "Scratching Experiments on Various Ceramic Materials," Philips Res. Repts. 30, 320 (1975).

9. B. R. Lawn and A. G. Evans, "A Model for Crack Initiation in Elastic/Plastic Indentation Field," J. Mat. Sci. 12, 2195-2199 (1977).

10. B. J. Hockey, "Plastic Deformation of Aluminum Oxide by Indentation and Abrasion," J. Am. Ceram. Soc. 54 [5] 223-231 (1971).

11. I. A. Cutter and R. McPherson, "Plastic Deformation of Al_2O_3 During Abrasion," J. Am. Ceram. Soc. 56 [5] 266-269 (1973).

12. M. V. Swain, "Microscopic Observations of Abrasive Wear of Polycrystalline Alumina," Wear, 35, 185-189 (1975).

13. R. L. Aghan and R. McPherson, "Mechanism of Material Removal During Abrasion of Rutile," J. Am. Ceram. Soc. 56 [1] 46-47 (1973).

14. E. D. Doyle and S. K. Dean, "The Fine Grinding of Glass and Ceramic Materials Using Conventional Grinding Wheels," pp. 107-114 in "Science of Ceramic Machining and Surface Finishing, II." Ed. B. J. Hockey and R. W. Rice. NBS Spec. Publ. 562, 1979.

15. A. G. Evans, "Abrasive Wear in Ceramics: An Assessment," pp. 1-14 in ref. [14].

16. A. G. Evans and D. B. Marshall, "Wear Mechanisms in Ceramics," pp. 439-453 in "Fundamental of Friction and Wear," Ed. D. A. Rigney, ASM, 1980.

17. B. R. Lawn and M. V. Swain, "Microfracture Beneath Point Indentations in Brittle Solids," J. Mat. Sci. 10, 113-122 (1975).

18. M. V. Swain, "Microfracture about Scratches in Brittle Solids," Proc. R. Soc. Lond. A366, 575-597 (1979).

19. B. R. Lawn, M. V. Swain and K. Phillips, "On the Mode of Chipping Fracture in Brittle Solids," J. Mat. Sci. 10, 1236-39 (1975).

20. R. Hill, "The Mathematical Theory of Plasticity," p. 97. Clarendon Press, Oxford, 1950.

21. A. G. Evans, "Fracture Toughness: The Role of Indentation Techniques," pp. 112-135 in "Fracture Mechanics Applied to Brittle Materials," Ed. S. W. Freiman, ASTM STP 678, 1979.

22. S. S. Chiang, D. B. Marshall and A. G. Evans, "The Response of Solids to Elastic/Plastic Indentation, I." J. Appl. Phys. 53 [1] 298-311 (1982).

23. B. K. Lawn, A. G. Evans and D. B. Marshall, "Elastic/Plastic Indentation Damage in Ceramics: The Median/Radial Crack System," J. Am. Ceram. Soc. 63 [9-10] 574-581 (1980).

24. M. V. Swain and J. T. Hagan, "Indentation Plasticity and the Ensuing Fracture of Glass. J. Phys. D, 9, 2201-14 (1976).

25. B. R. Lawn, "A Model for the Wear of Brittle Solids under Fixed Abrasive Conditions," Wear, 33, 369-372 (1975).

26. O. Imanaka, S. Fujino and S. Mineta, "Direct Observation of Material Removal Process During Grinding of Ceramics by Micro-Flash Technique," pp. 37-43 in "Science of Ceramic Machining and Surface Finishing," Ed. S. J. Schneiders, Jr. and R W. Rice, NBS Spec. Publ. 348, 1972.

27. A. G.Evans and T. R. Wilshaw, "Quasi-Static Solid Particle Damage in Brittle Solids, I," Acta Met. 24, 939-956 (1976).

28. A. Arora, D. B. Marshall, B. R. Lawn and M. V. Swain, "Indentation Deformation/Fracture of Normal and Anomalous Glasses," J. Non-Cryst. Solids, 31, 415-428 (1979).

29. J. T. Hagan, "Cone Crack Around Vickers Indentations in Fused Silica Glass," J. Mat. Sci., 14, 462-466 (1979).

30. J. T. Hagan, "Shear Deformation Under Pyramidal Indentation in Soda-Lime Glass," J. Mat. Sci., 15, 1412-24 (1980).

31. F. M. Ernsberger, "Mechanical Properties of Glass," J. Non-Cryst. Solids, 25 [1-3] 293-321 (1977).

32. K. W. Peter, "Densification and Flow Phenomena of Glass in Indentation Experiments," Non-Cryst. Solids 5, 103-115 (1970).

33. M. V. Swain, "Crack Nucleation About Pointed Indentations in Glass," J. Am. Ceram. Soc. 62 [5-6] 318-319 (1979).

34. J. T. Hagan, "Micromechanics of Crack Nucleation During Indentation," J. Mat. Sci. 14, 2975-80 (1979).

35. J. T. Hagan and M. V. Swain, "The Origin of Median and Lateral Cracks Around Plastic Indents in Brittle Materials," J. Phys. D., 11, 2091-2102 (1978).

36. M. Ernsberger, "Tensile and Compressive Strength of Pristine Glasses by an Oblate Bubble Technique," Phys. Chem. Glasses, 10 [6] 240-45 (1969).

37. D. B. Marshall and B. R. Lawn, "Residual Stress Effects in Sharp Contact Cracking, I," J. Mat. Sci. 14 [8] 2001-12 (1979).

38. J. J. Petrovic, R. A. Dirks, L. A. Jacobson and M. G. Mendiratta, "Effects of Residual Stresses on Fracture from Controlled Surface Flaws," J. Am. Ceram. Soc., 59 [3-4] 177-178 (1976).

39. B. R. Lawn and D. B. Marshall, "Residual Stress Effects in Failure from Flaws, "J. Am. Ceram. Soc., 62 [1-2] 106-108 (1979).

40. D. B. Marshall, B. R. Lawn and P. Chantikul, "Residual Stress Effects in Sharp Contact Cracking, II," J. Mat. Sci. 14 [9], 2225-35 (1979).

41. D. B. Marshall and B. R. Lawn, "Flaw Characteristics in Dynamic Fatigue: The Influence of Residual Contact Stresses," J. Am. Ceram. Soc., 63 (9-10) 532-26 (1980).

42. B. R. Lawn, K. Jakus and A. C. Gonzalez, "Sharp vs. Blunt Crack Hypotheses in the Strength of Glass: A Critical Study Using Indentation Flaws," J. Am. Ceram. Soc. 68 [1] 25-34 (1985).

43. P. Chantikul, G. R. Anstis, B. R. Lawn and D. B. Marshall, "A Critical Evaluation of Indentation Techniques for Measuring Fracture Toughness: II," J. Am. Ceram. Soc., 64 (9) 539-543 (1981).

44. B. R. Lawn, D. B. Marshall and P. Chantikul, "Mechanics of Strength Degrading Contact in Silicon," J. Mat. Sci., 16 (7) 1769-75 (1981).

45. R. W. Rice, J. J. Mecholsky, Jr. and P. F. Becher, "The Effect of Grinding Direction on Flaw Character and Strength of Single Crystal and Polycrystalline Ceramics," J. Mat. Sci. 16 (4) 853-62 (1981).

46. C. A. Anderson and R. J. Bratton, "Effect of Surface Finish on the Strength of Hot Pressed Silicon Nitride," pp. 463-474 in "Science of Ceramic Machining and Surface Finishing, II," ed. B. J. Hockey and R. W. Rice, NBS Spec. Publ. 562, 1979.

47. G. R. Anstis, P. Chantikul, B. R. Lawn and D. B. Marshall, "A Critical Evaluation of Indentation Techniques for Measuring Fracture Toughness: I. Direct Crack Measurements," J. Am. Ceram. Soc., 64 (9) 534-38 (1981).

48. R. G. Hoagland, C. W. Marshall and H. Duckworth, "Reduction of Errors in Ceramics Bend Tests," J. Am. Ceram. Soc. 59 (5-6) 189-192 (1976).

49. B. R. Lawn and E. R. Fuller, "Equilibrium Penny-like Cracks in Indentation Fracture," J. Mat. Sci. 10, 2016-24 (1975).

50. S. Timoshenko, "Strength of Materials," Part 2, Ch. V, Van Nostrand Co. Princeton, 1956.

51. B. R. Lawn, "The Indentation Crack As a Model Surface Flaw," pp. 1-25 in "Fracture Mechanics of Ceramics," v. 5, Ed. R. C. Bradt, A. G. Evans, D. P. H. Hasselman and F. F. Lange. Plenum Press, New York, 1983.

52. R. R. Cook, B. R. Lawn and G. R. Anstis, "Fatigue Analysis of Brittle Materials Using Indentation Flaws, Part 2. Case Study on a Glass-Ceramic," J. Mat. Sci. 17, 1108-16 (1982).

53. B. R. Lawn, T. Jensen and A. Arora, "Brittleness as an Indentation Size Effect," J. Mat. Sci. 11, 573-575 (1976).

54. D. B. Marshall and B. R. Lawn, "Residual Stresses in Dynamic Fatigue of Abraded Glass," J. Am. Ceram. Soc. 64 [1] C6-7 (1981).

FIGURE CAPTIONS

Fig. 1. Schematic illustrating the residual stress fields associated with a non-uniform plastic layer created by machining and the associated sub-surface machining flaws.

Fig. 2. Indentation cracks revealed in (a) as-received and (b) machined specimens using a dye penetrant.

Fig. 3. Trends in indentation crack radius with indentation load for as-received (and pre-annealed) specimens and for machined specimens at two different depths of cut.

Fig. 4. Cumulative distributions of indentation crack radius (normalized by load) for as-received and machined (2 μm depth of cut) specimens.

Fig. 5. An optical micrograph of an indentation crack in a machined specimen revealing the non-uniformity of the crack pattern.

Fig. 6. Effects of annealing, after machining (10 μm depth of cut), on the indentation crack radius, compared with values for as-received specimens (P = 9.8 N).

Fig. 7. Relative precursor crack growth, $(C_m-C_i)/C_i$, as a function of indentation load for as-received and machine samples. The data range is represented by the bands.

Fig. 8. The reduction in precursor crack growth ($\Delta C/C_i$) in as-received, indented specimens after annealing (indentation load, 40N).

Fig. 9. A comparison of the trend in the average strength of indented specimens in the as-received and machined states. The band indicates the variation in the average strengths of as-received indented specimens amongst batches of material.

Fig. 10. The effects of annealing (for 24h at 520°C), after indentation, on the average strengths of machined specimens (5 μm depth of cut).

Fig. 11. The effects of annealing for 2h on the strength of as-received, indented specimens.

Fig. 12. (a) SEM micrograph of a machined surface (5 μm depth of cut) at a higher magnification.

(b) Chipped region by indentation in machined surface (5 μm depth of cut), showing the morphological similarity between machined surfaces and the chipped region by indentation.

Fig. 13. SEM micrograph of machined surfaces at various depths of cut.

Fig. 14. Profiles of machined surface (5 μm depth of cut) before (a) and after HF etching (b).

Fig. 15. SEM cross-sectional view of a etched, machined surface.

Fig. 16. Profiles of (a) as-received surface and (b) machined surface of same specimen after etching.

Fig. 17. Indentation cracks in (a) as-received and (b) machined surfaces (depth of cut 2 μm).

Fig. 18. An optical micrograph of an indentation crack formed at low load indicating the irregularity in crack path on the machined surface (20 μm depth of cut).

Fig. 19. Comparison of indentation cracks at lower load in (a) as-received and (b) machined surfaces (depth of cut 2 μm).

Fig. 20. SEM micrographs of fracture surfaces revealing the tension edge of (a) as-received specimen and (b) machined specimen (2 μm depth of cut).

Fig. 21. SEM micrographs of tension edges of fracture of machined specimens (5 μm depth of cut) showing (a) undulations of machined surface and (b) breaking away of edges.

Fig. 22. Edges between fracture surfaces and the machined surfaces: (a) 20 μm, (b) 2μm depth of cut.

Fig. 23. An optical micrograph of an indentation crack formed at 78.5N load, showing chipping by lateral crack propagation.

Fig. 24. An optical micrograph of an dummy indentation crack (P = 49N) before (a) and after strength test (b) and seven months later (c), showing the slow growths of radial and lateral crack as well as the precursor crack growth during strength test.

Fig. 25(a). Schematic illustrating the buckling occurs at incidence and propagation of lateral crack of indentation.

(b). The effects on buckling around indentation when induced in machined surface.

Fig. 26. Plot of indentation/strength parameter $SP^{1/3}$ against indentation load P of as-received and machined specimens.

Fig. 27. Plot of strength of indented machined specimens against the initial length of the dominant indentation crack for specimens that fail from indentation cracks. The data represent the mean and standard deviation of at least 6 measurements. The line represents a prediction from the strength/flaw-size equation $K_c = (2/\sqrt{\pi})\ S\sqrt{C_i}$ with a fracture toughness representative of soda-lime glass, $K_c = 0.75\ \mathrm{MPa.m}^{1/2}$.

Fig. 28. Plots of applied stress against crack radius for indentation cracks (P = 49N) in glass. Flaws in the post-indentation and annealed states (superscripts o and A, respectively) are plotted in dashed lines and represent limiting states. The trend pertinent to the as-received and machined specimens investigated in this study are plotted as the solid and dotted lines respectively.

Fig. 29. Plot of $P/C_i^{3/2}$ against indentation load P for as-received and machined glass, showing the higher values of machined specimens over the constant $P/C_i^{3/2}$ for as-received specimens.

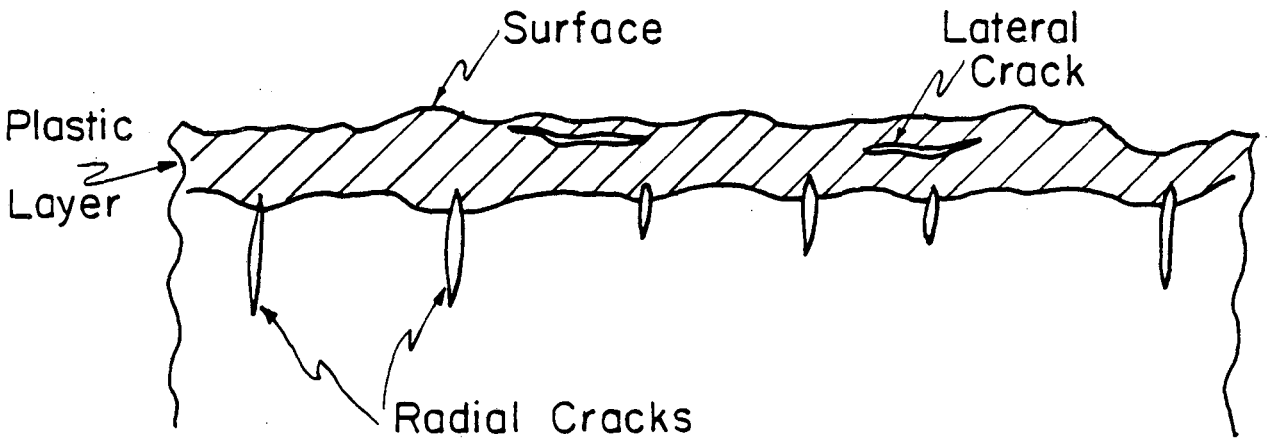

a) MACHINING DAMAGE

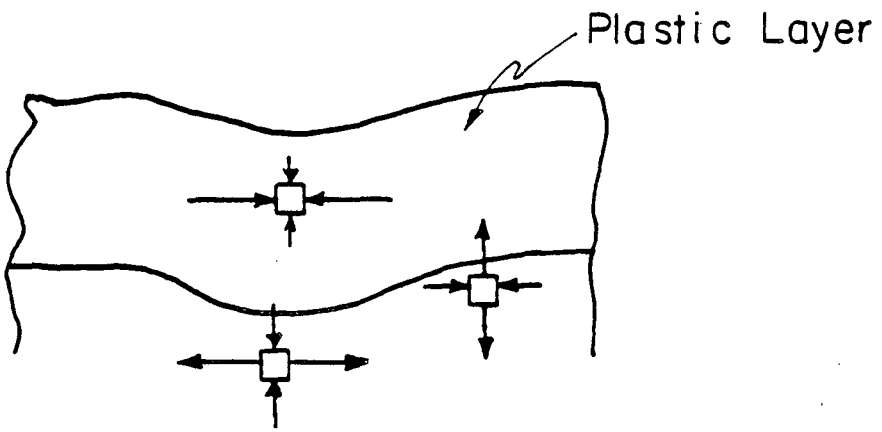

b) RESIDUAL STRESS DISTRIBUTION

XBL855-6255

Fig. 1

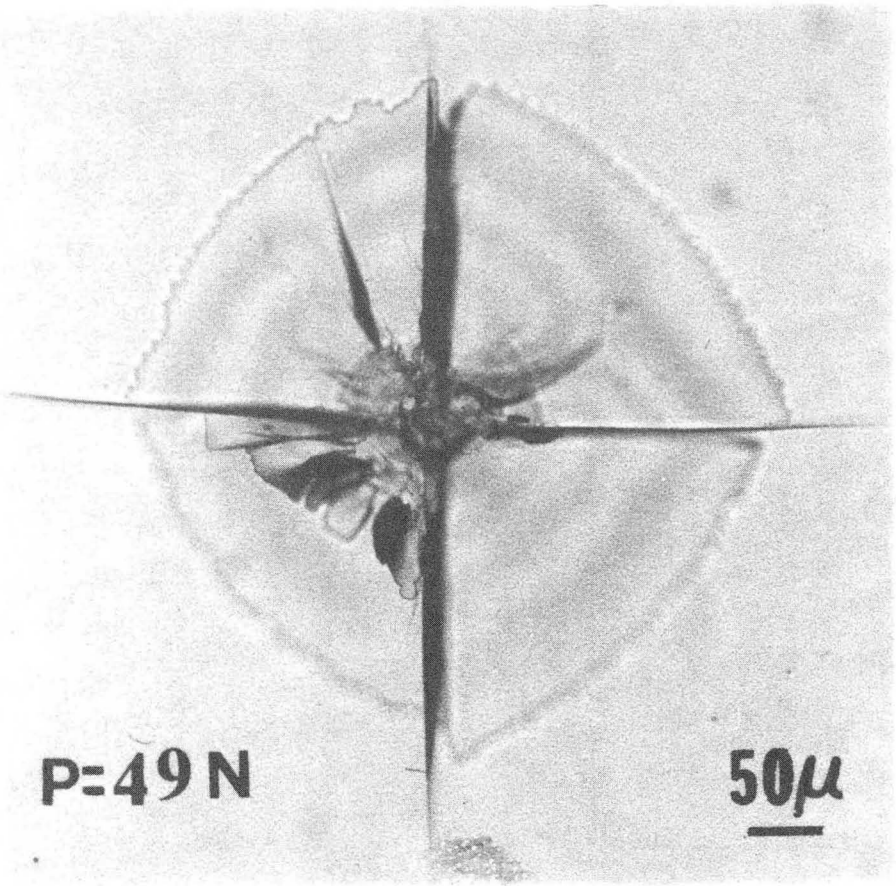

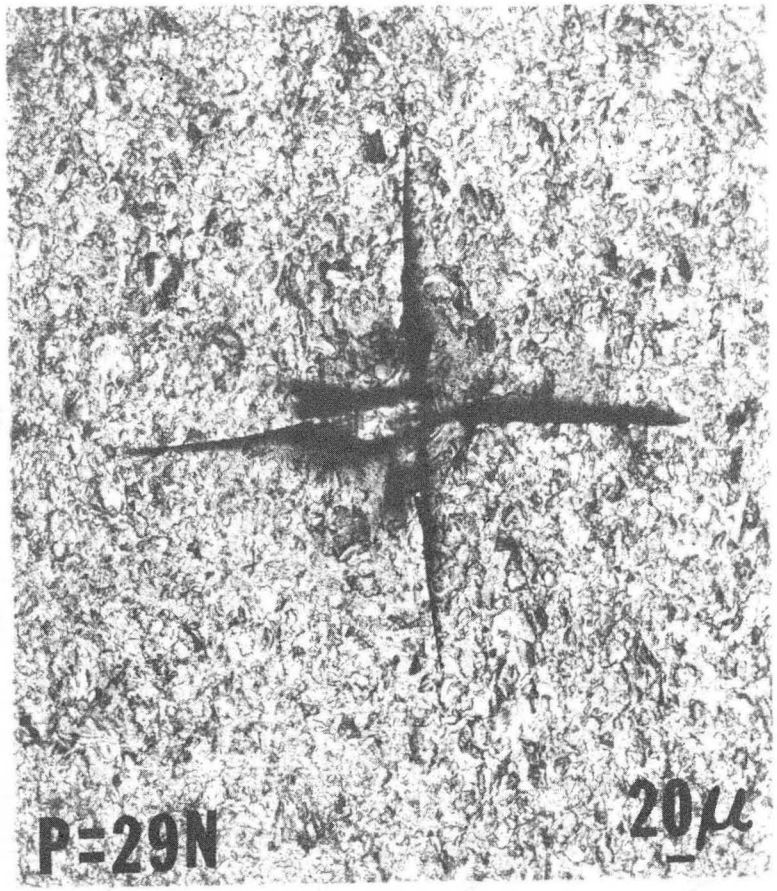

XBB 855-3962

Fig. 2

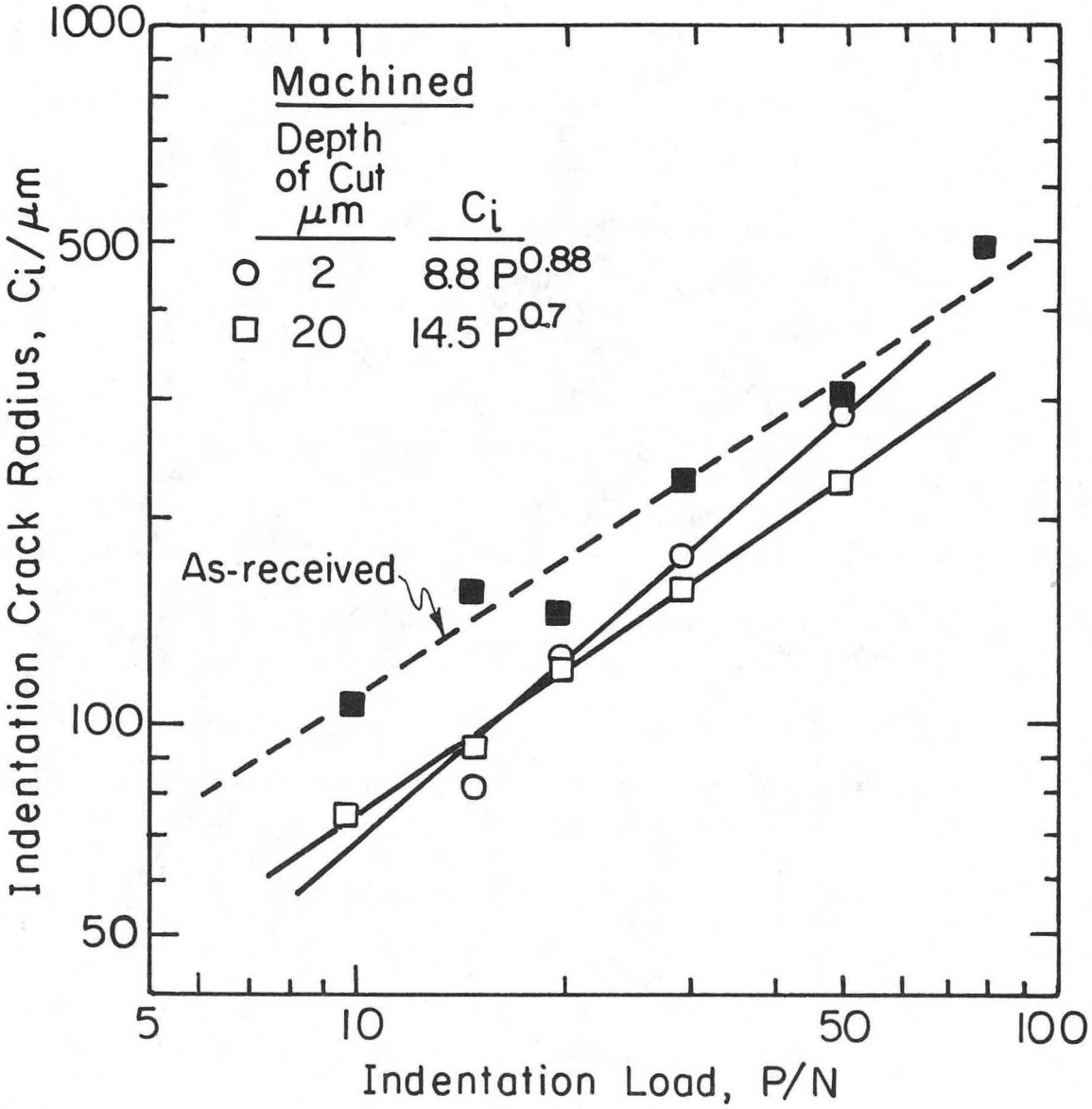

XBL 853-6003A

Fig. 3

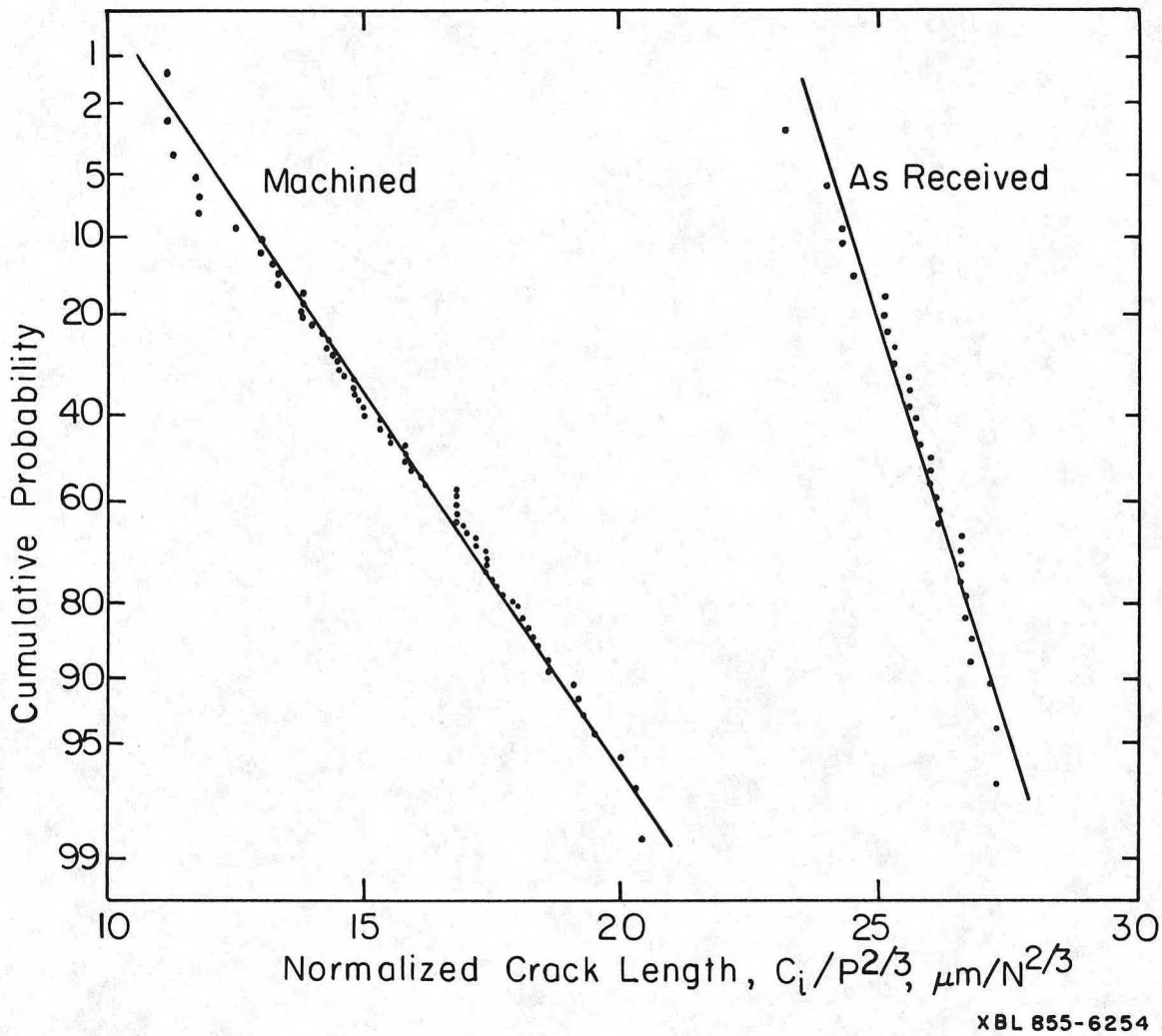
Machined
As Received
Cumulative Probability
1
2
5
10
20
40
60
80
90
95
99
10
15
20
25
30
Normalized Crack Length, $C_i/P^{2/3}$, $\mu m/N^{2/3}$
XBL 855-6254

Fig. 4

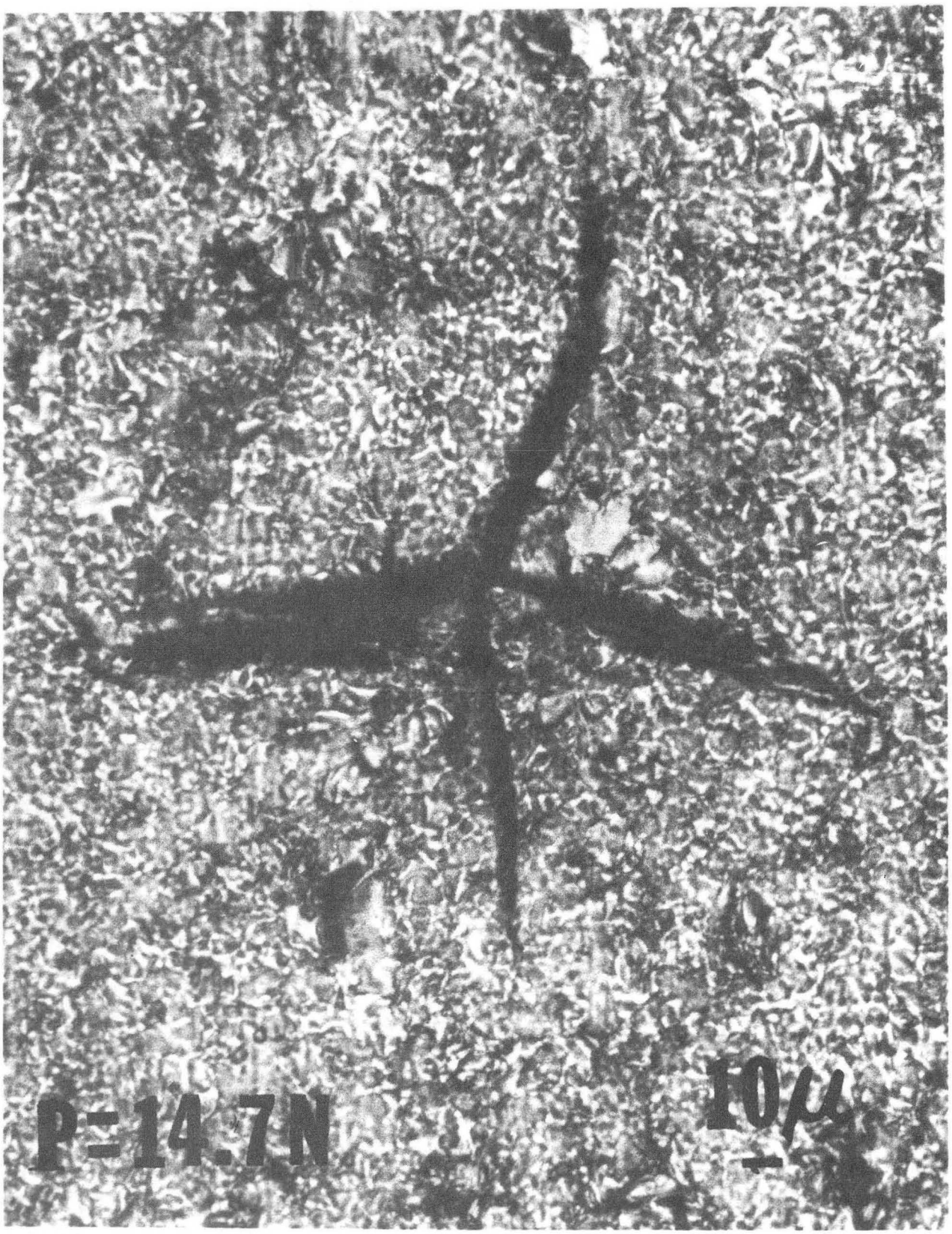

XBB 855-3965

Fig. 5

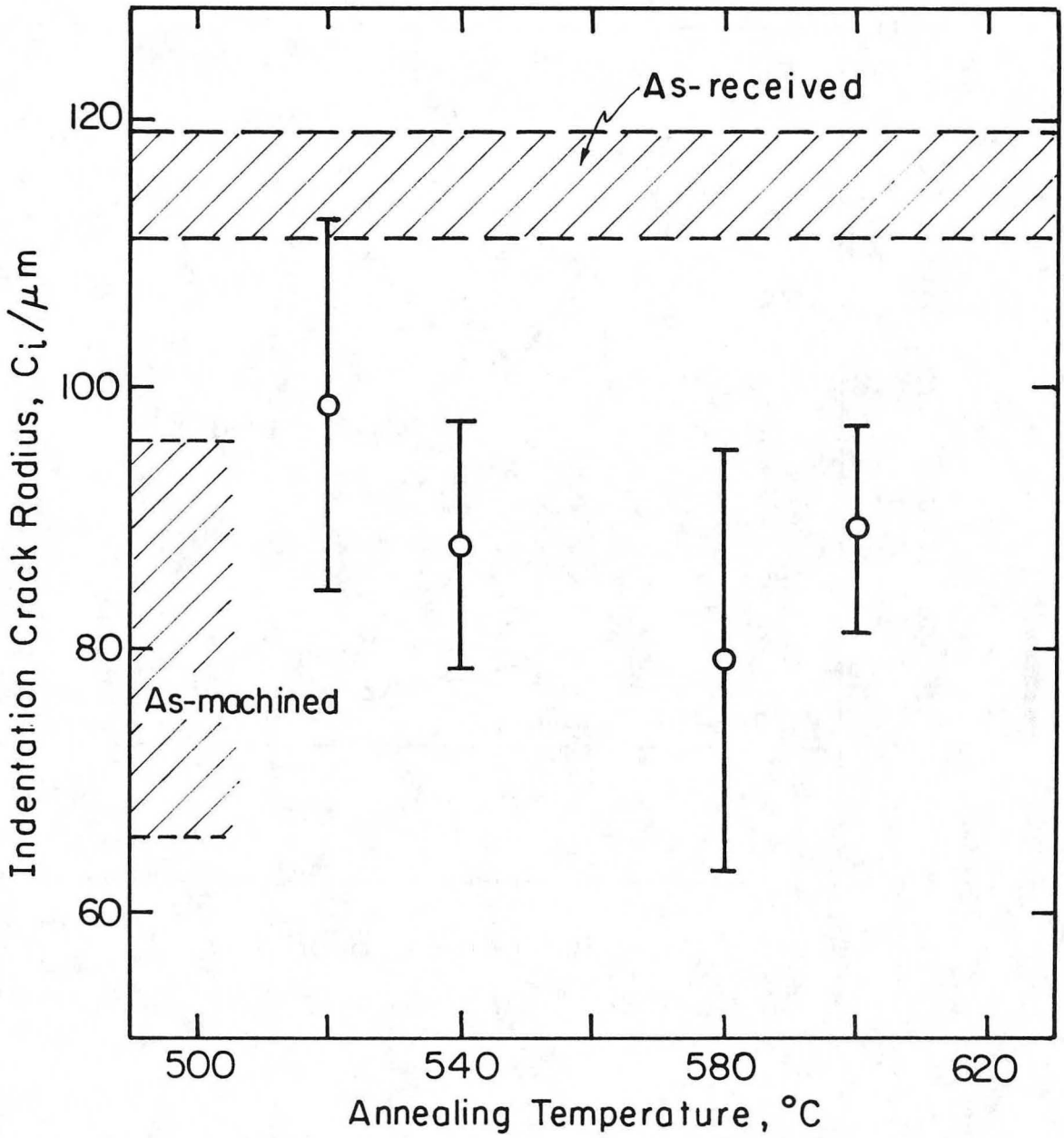

Fig. 6

XBL 855-6256A

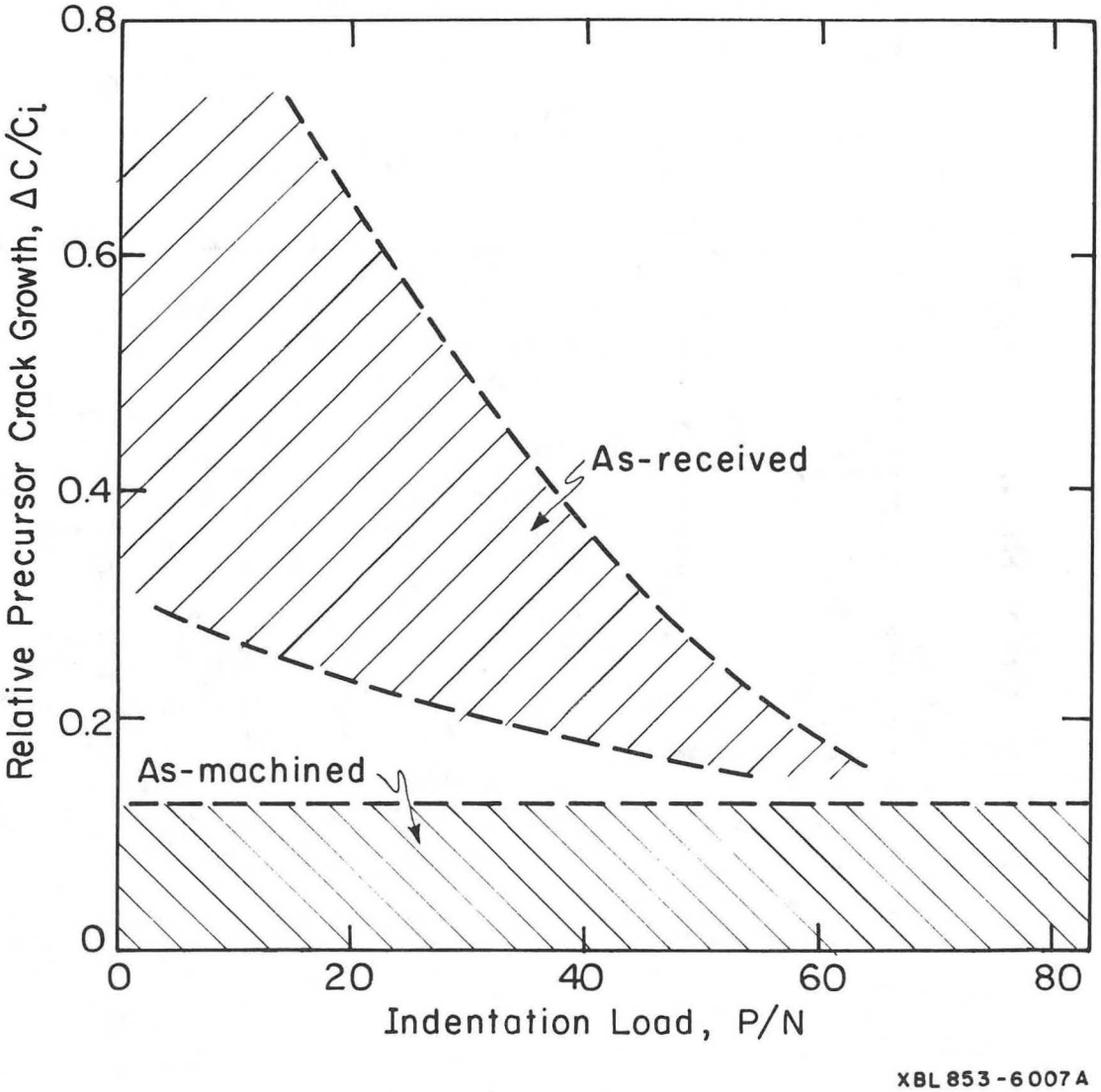
0.8
0.6
0.4
0.2
0
Relative Precursor Crack Growth, ΔC/Ci
As-received
As-machined
0
20
40
60
80
Indentation Load, P/N
XBL 853-6007A

Fig. 7

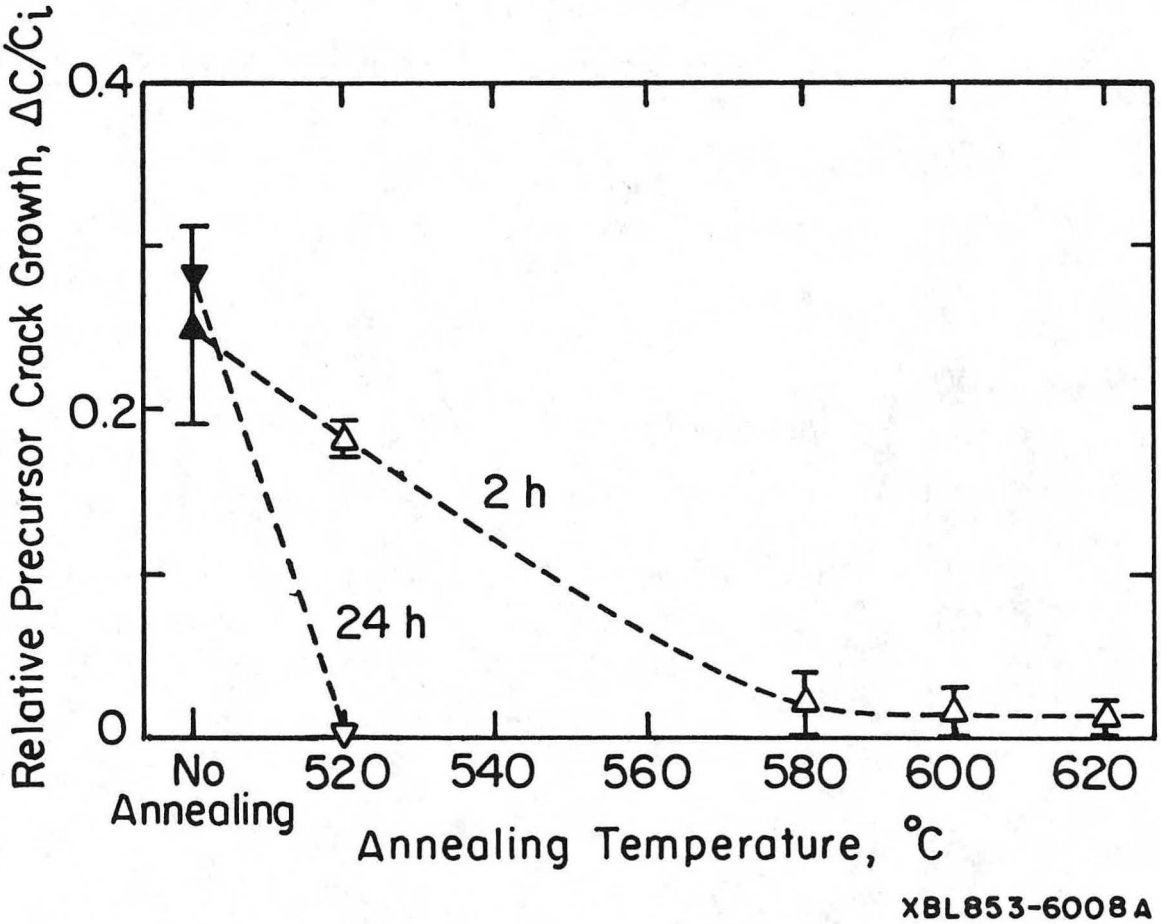
Relative Precursor Crack Growth, ΔC/Ci
0.4
0.2
0
2 h
24 h
No Annealing
520
540
560
580
600
620
Annealing Temperature, °C
XBL853-6008A

Fig. 8

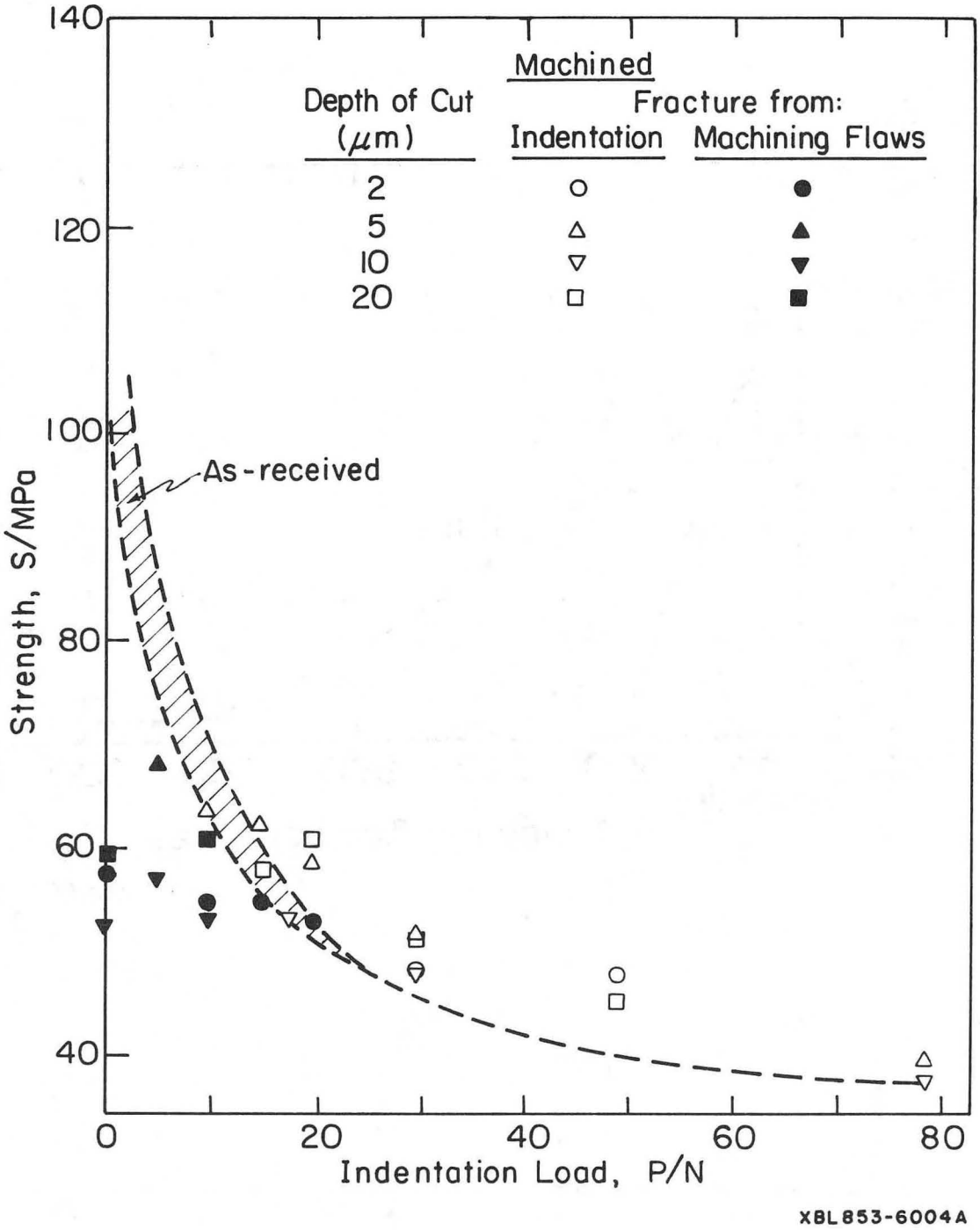
Machined
Depth of Cut (μm)
Fracture from:
Indentation
Machining Flaws
2
5
10
20
As-received
Strength, S/MPa
Indentation Load, P/N
140
120
100
80
60
40
0
20
40
60
80
XBL853-6004A

Fig. 9

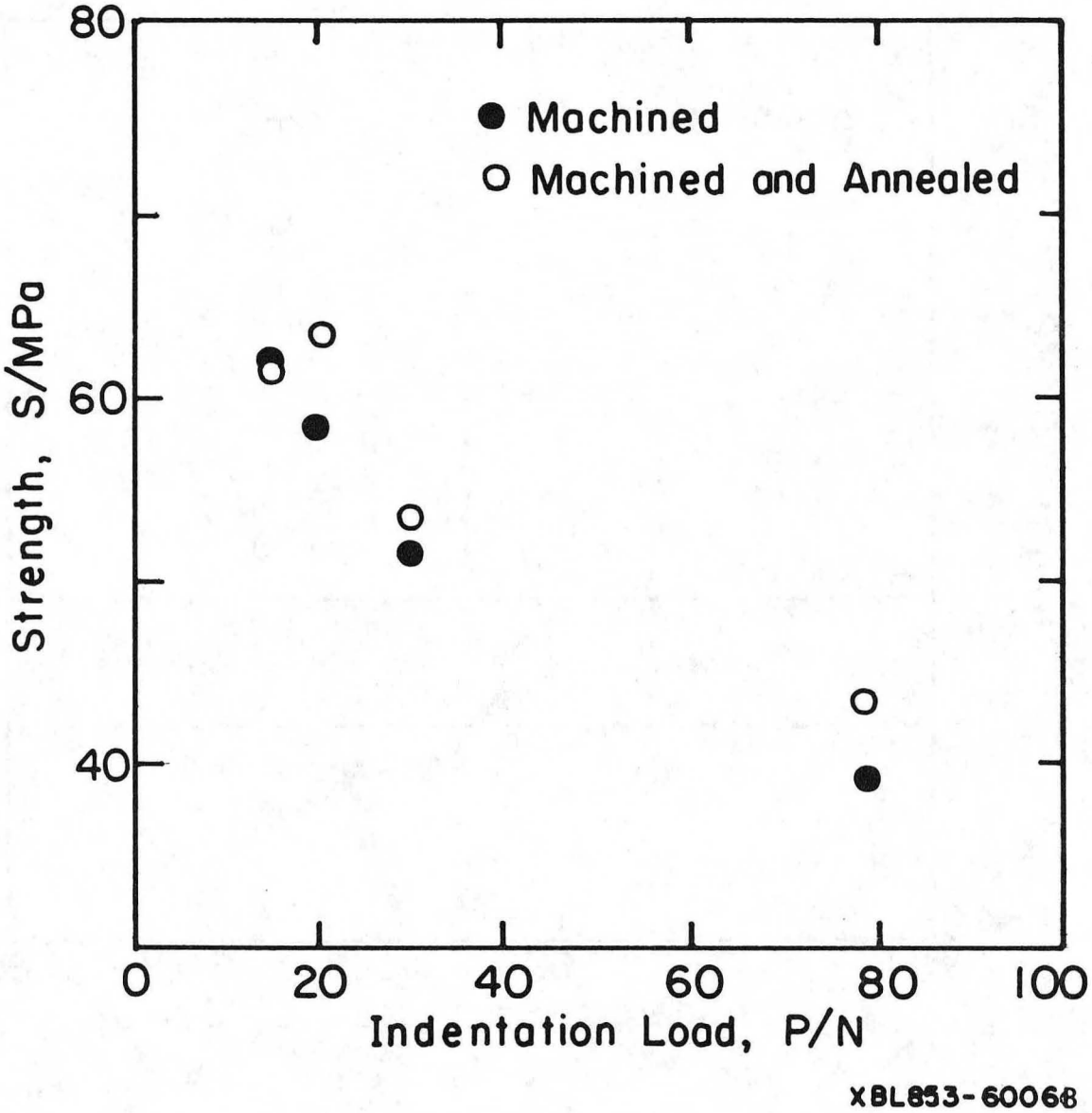
80
60
40
Strength, S/MPa
Machined
Machined and Annealed
0
20
40
60
80
100
Indentation Load, P/N
XBL853-60068

Fig. 10

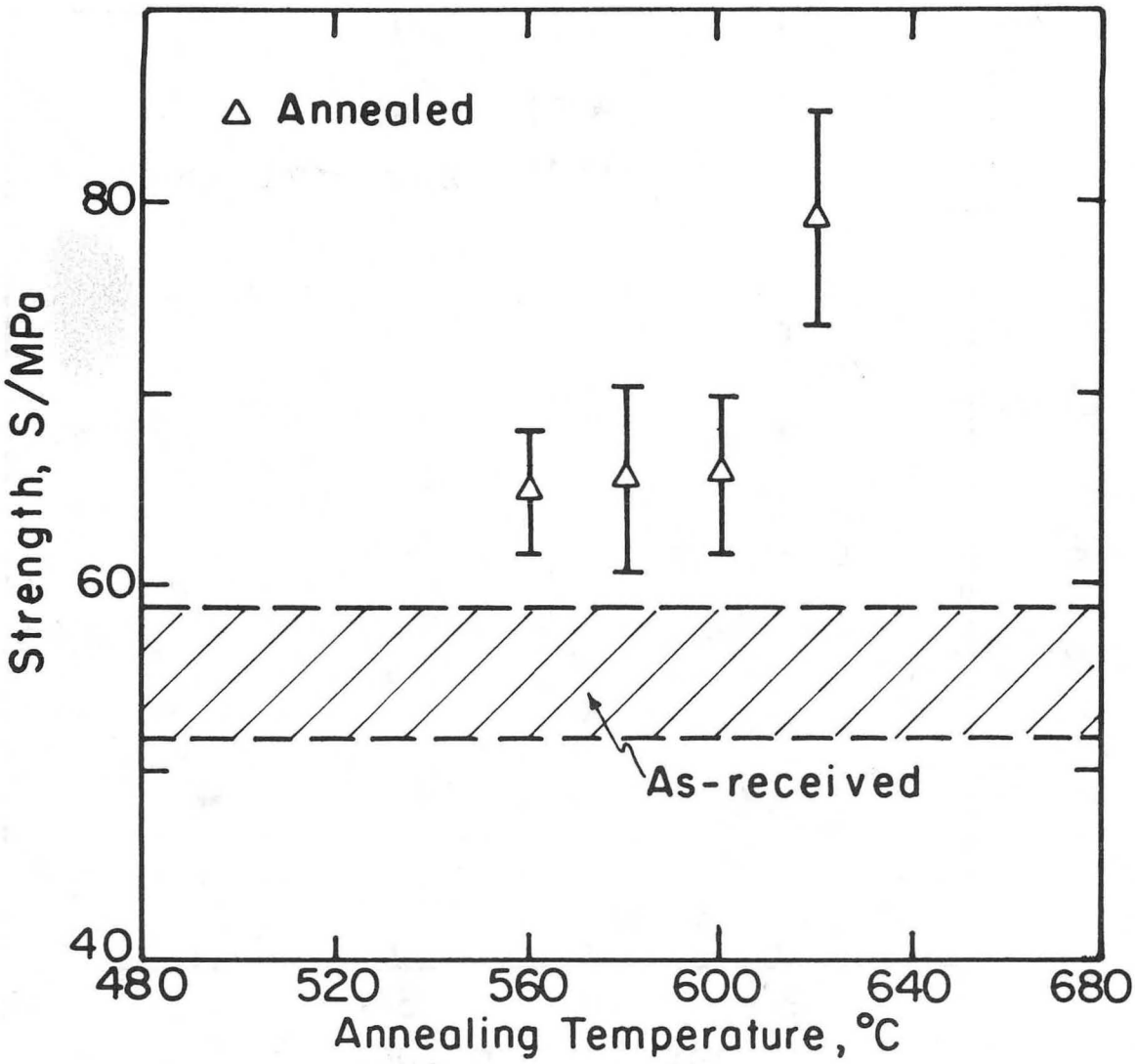

XBL853-6005B

Fig. 11

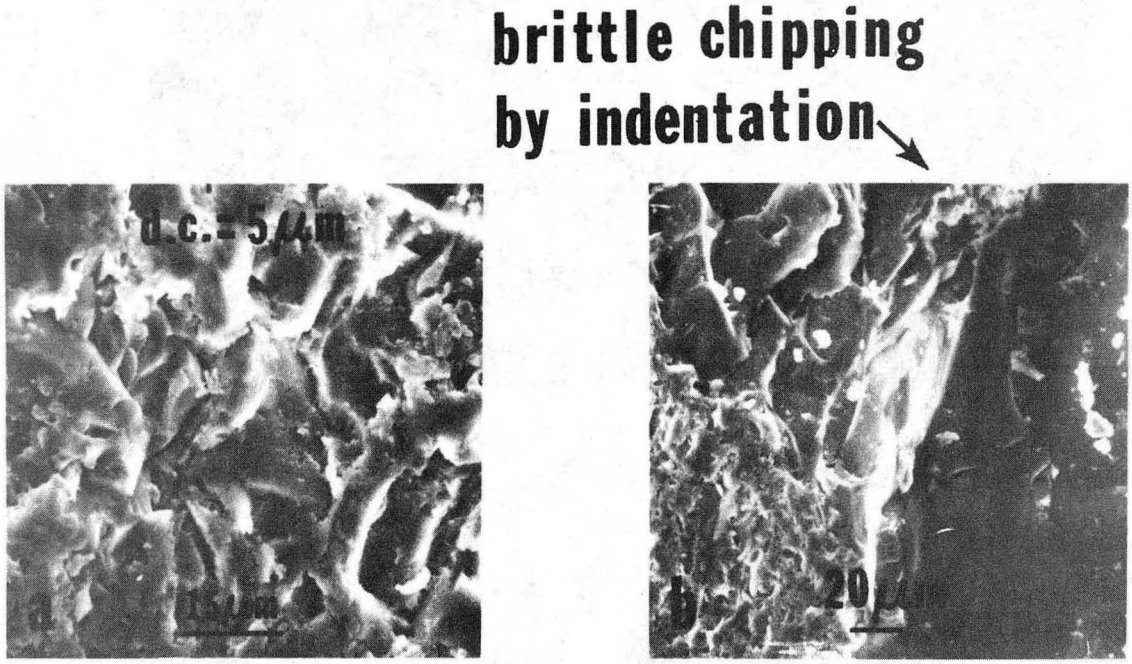

XBB 858-6754

Fig. 12

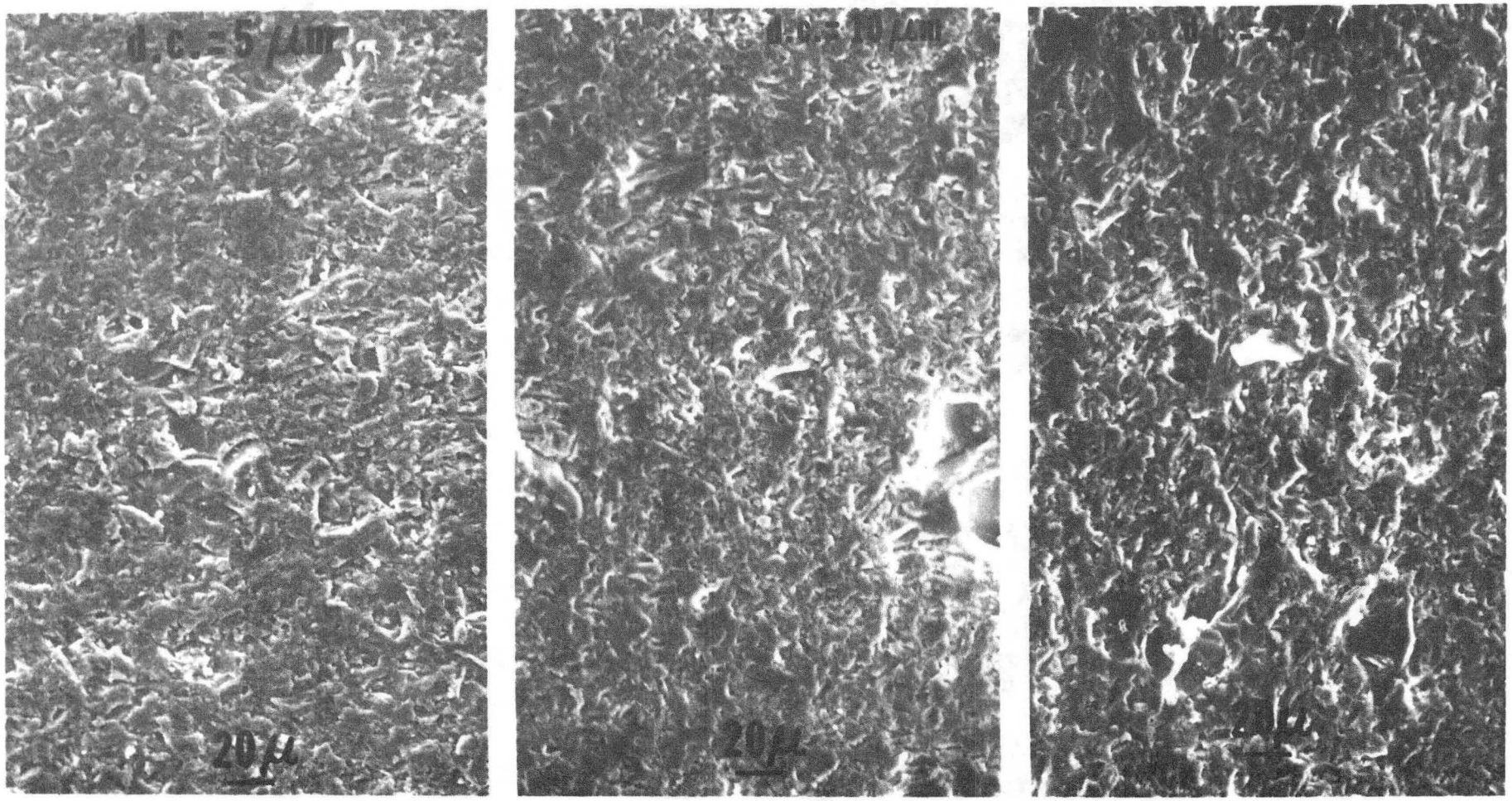

XBB 858-6753

Fig. 13

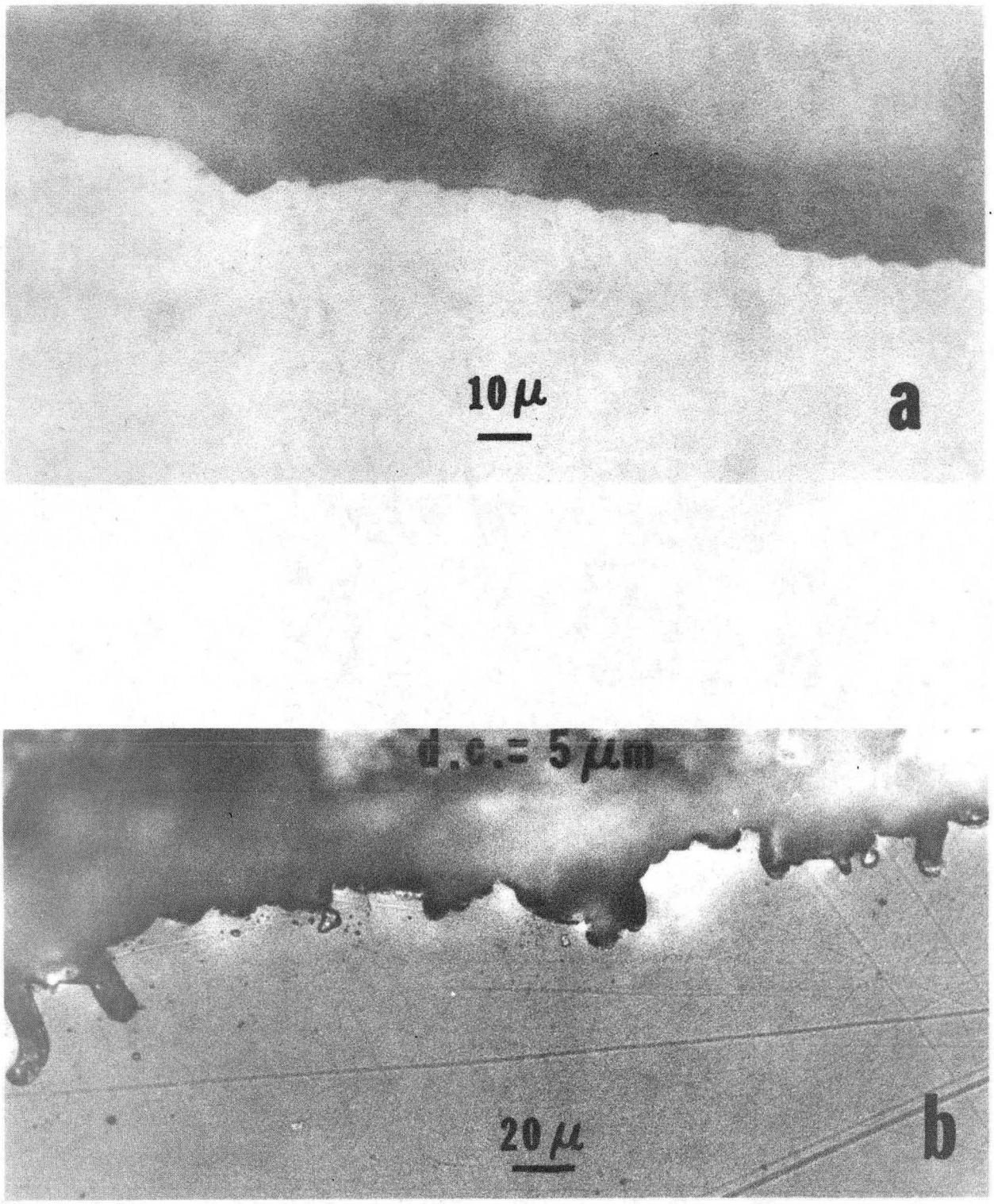

XBB 855-3967

Fig. 14

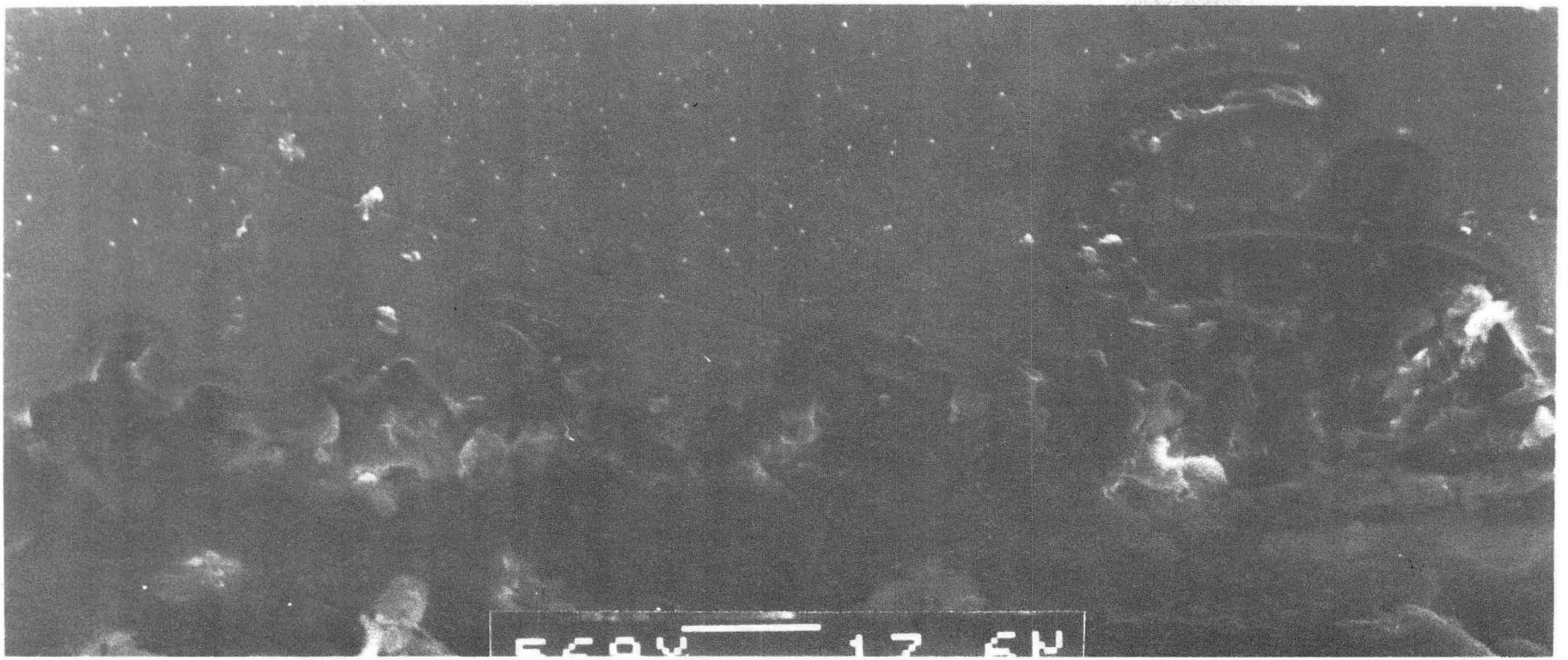

XBB 858-6751

Fig. 15

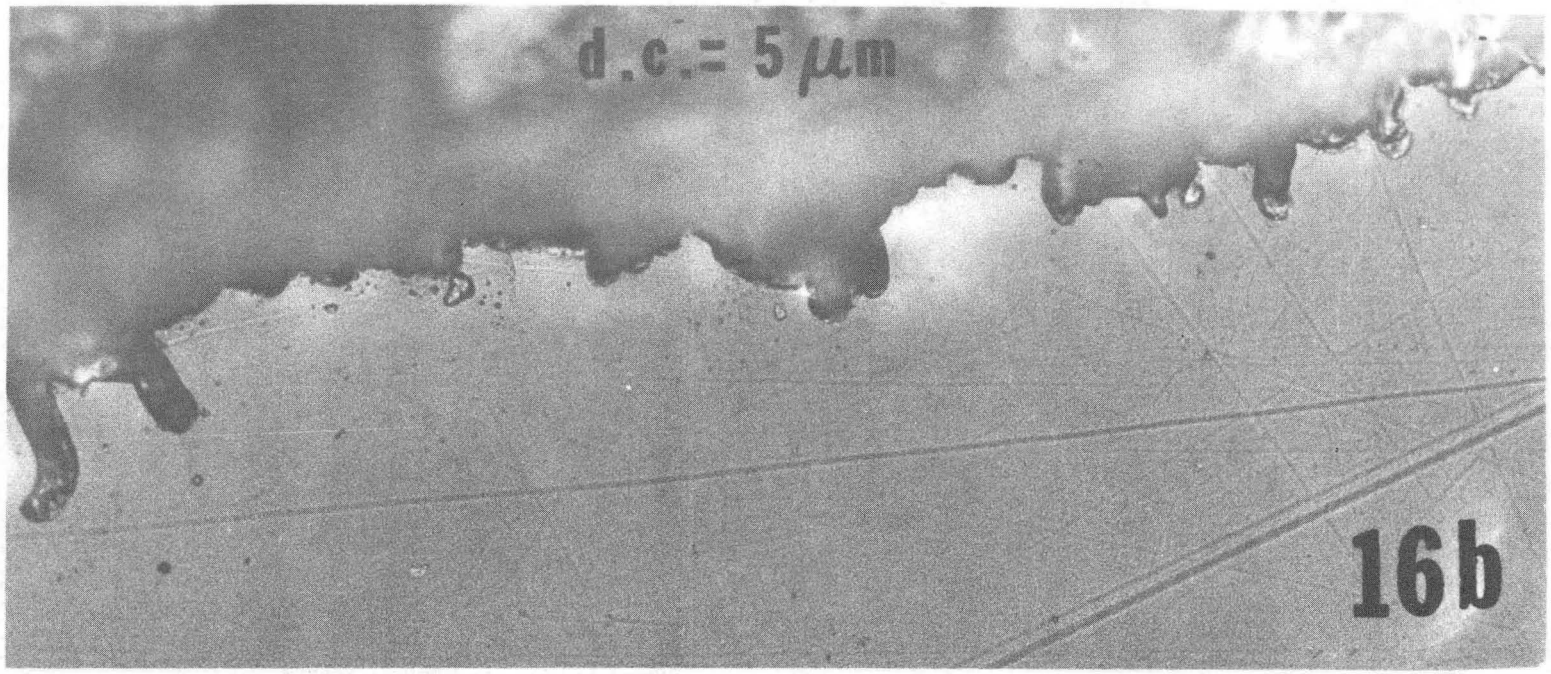

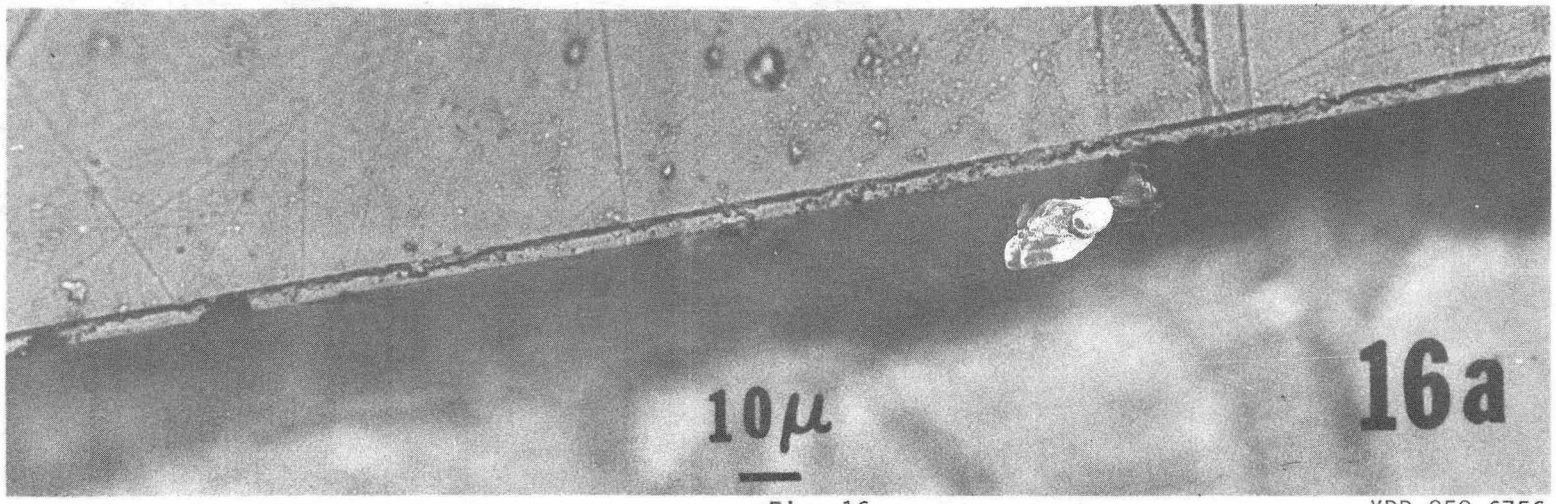

Fig. 16

XBB 858-6756

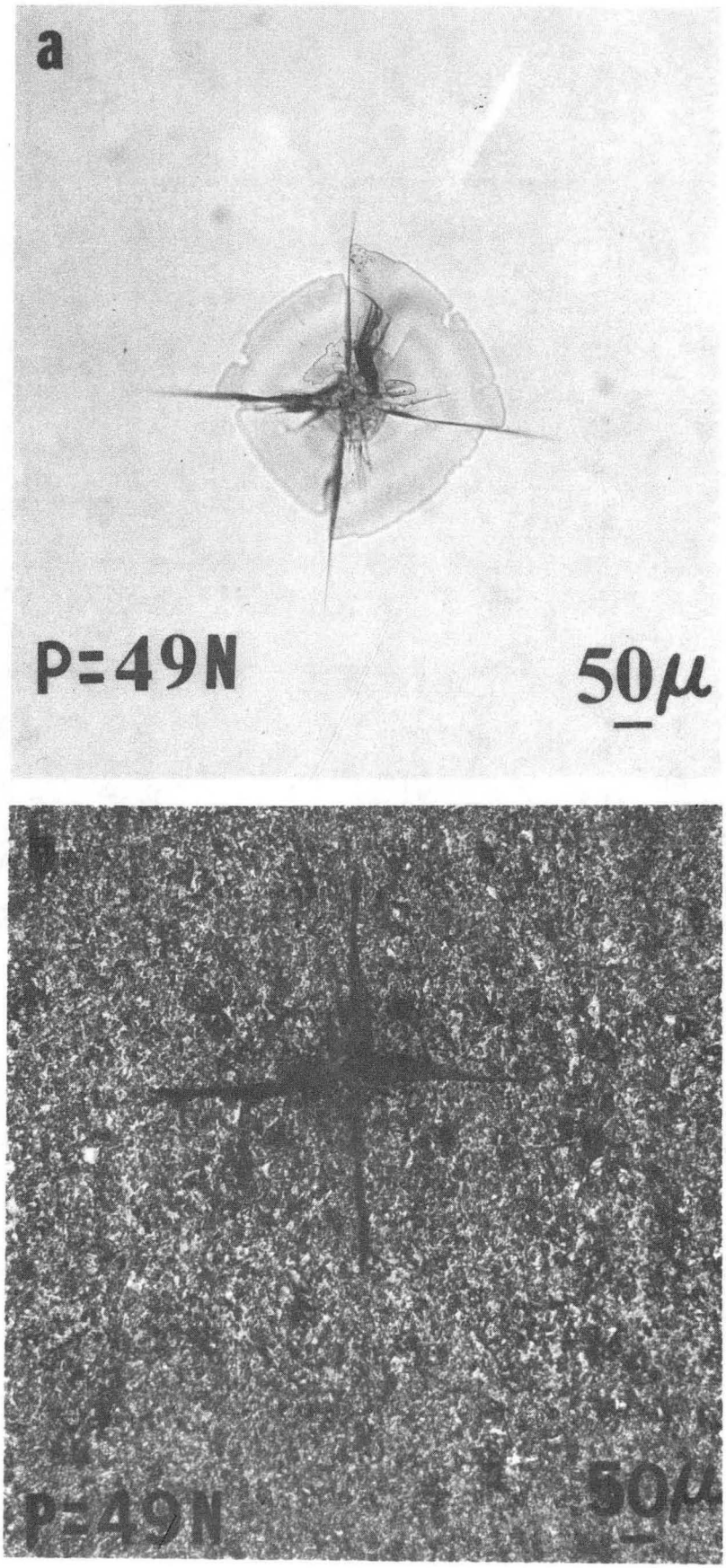

XBB 858-6757

Fig. 17

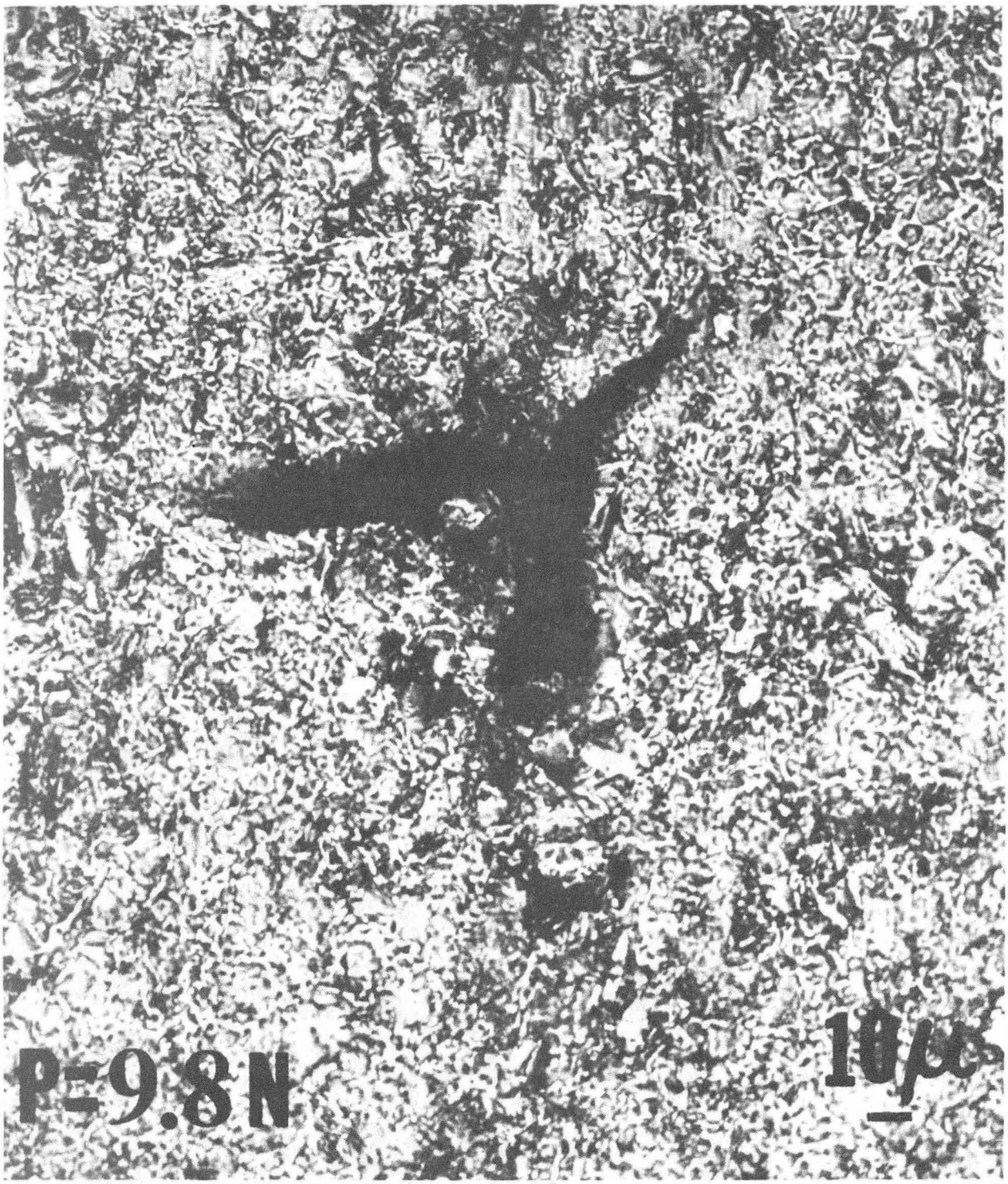

XBB 855-3966

Fig. 18

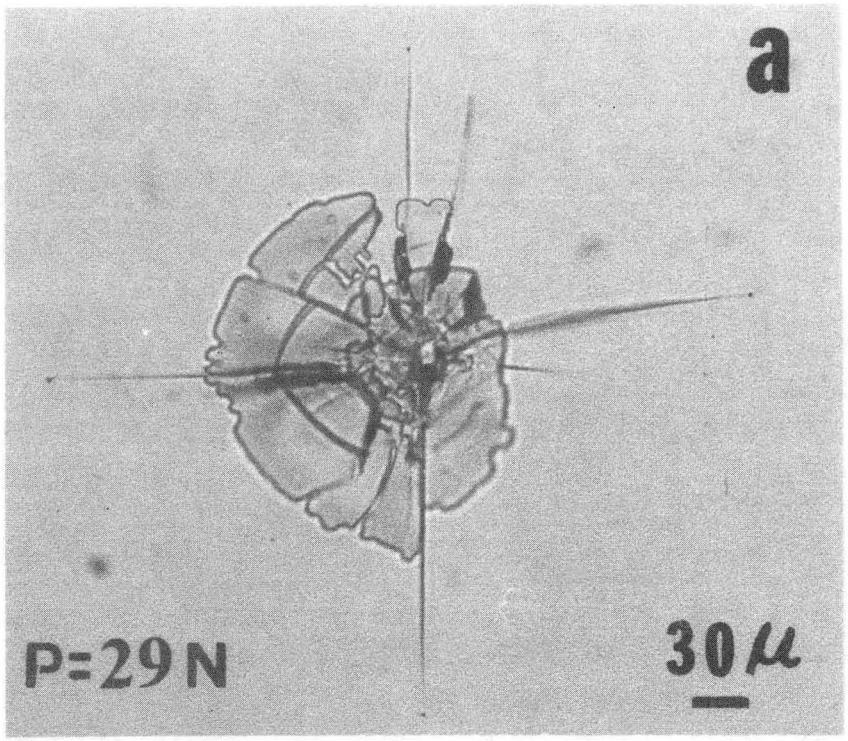

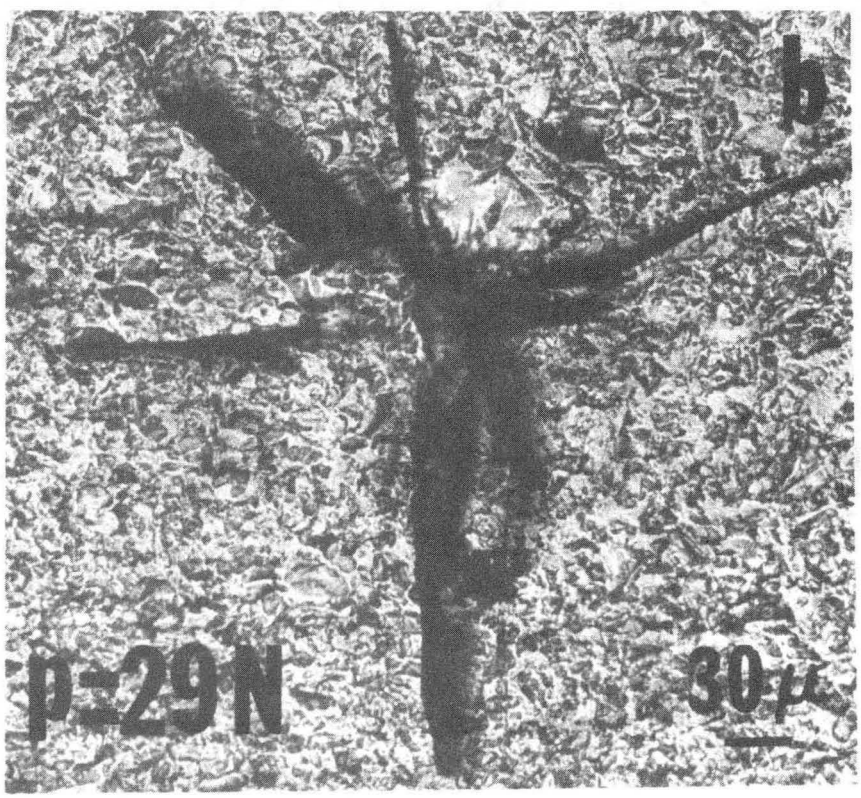

XBB 858-6755

Fig. 19

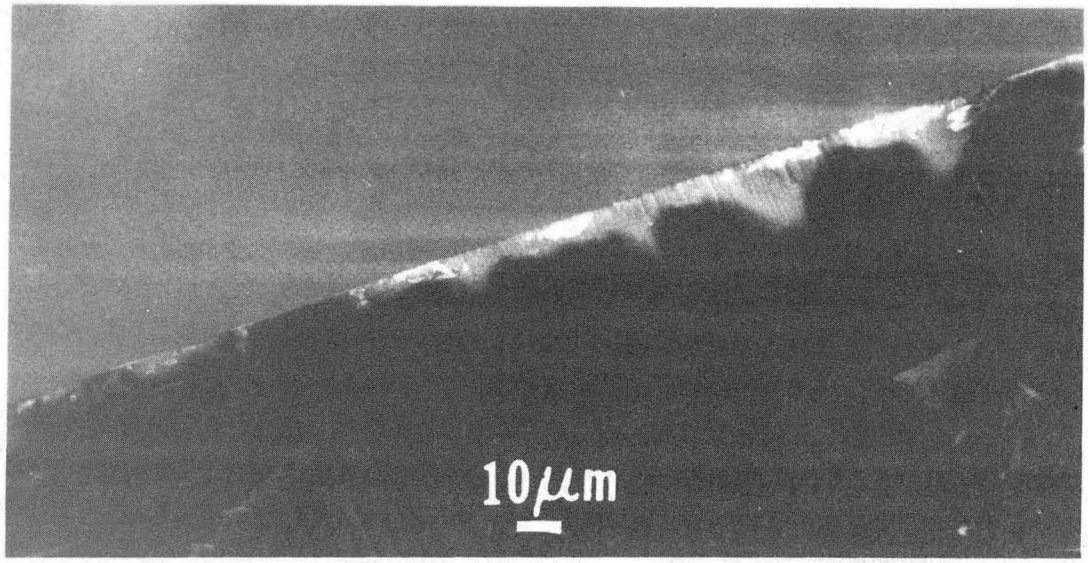

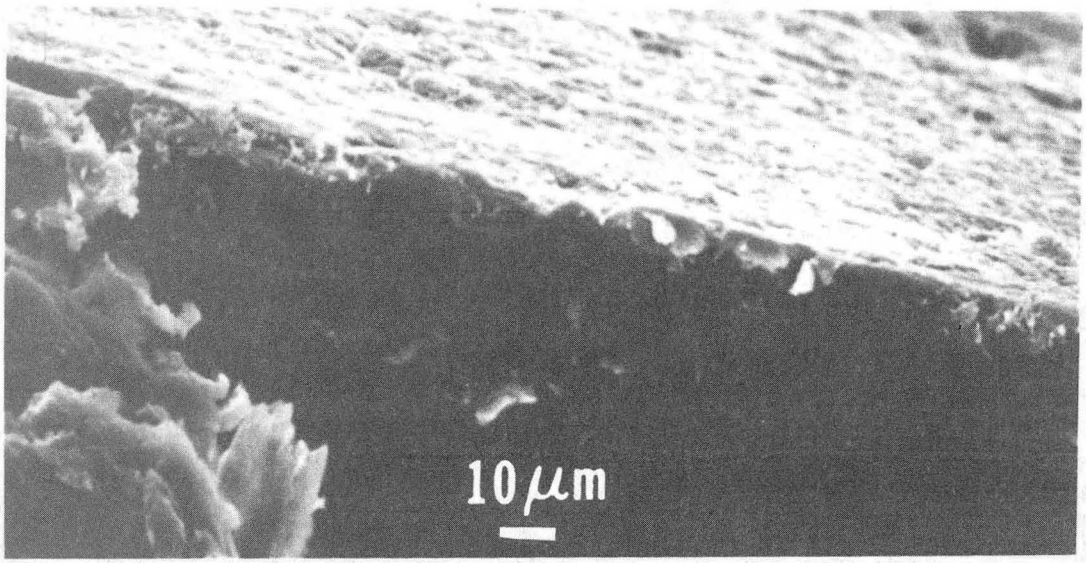

XBB 850-9214

Fig. 20

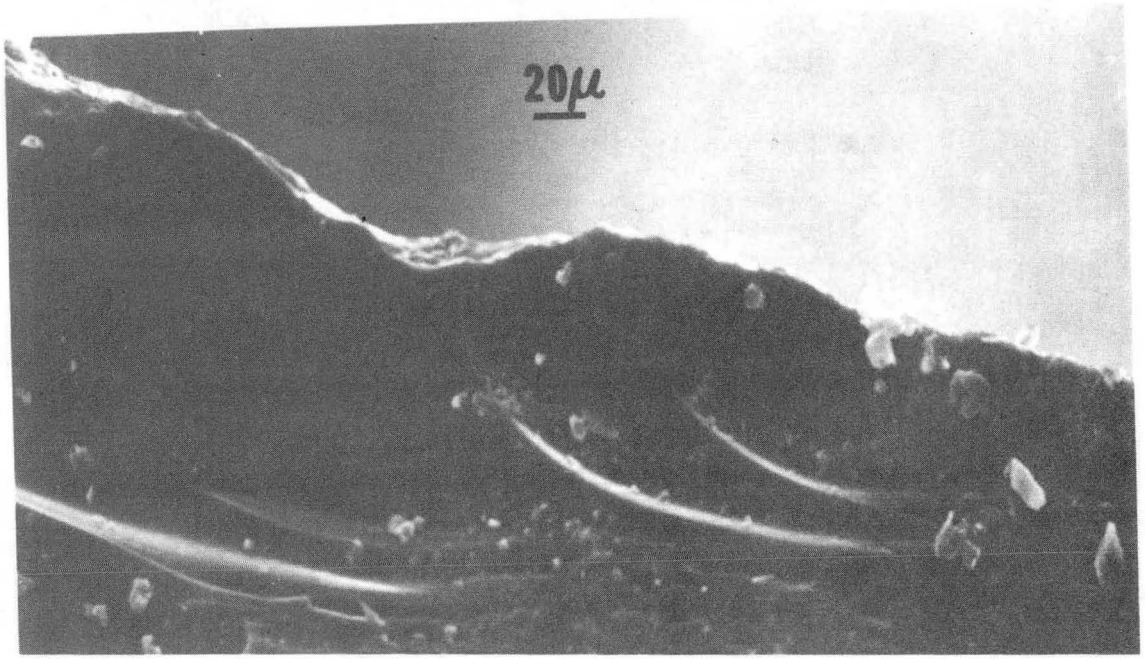

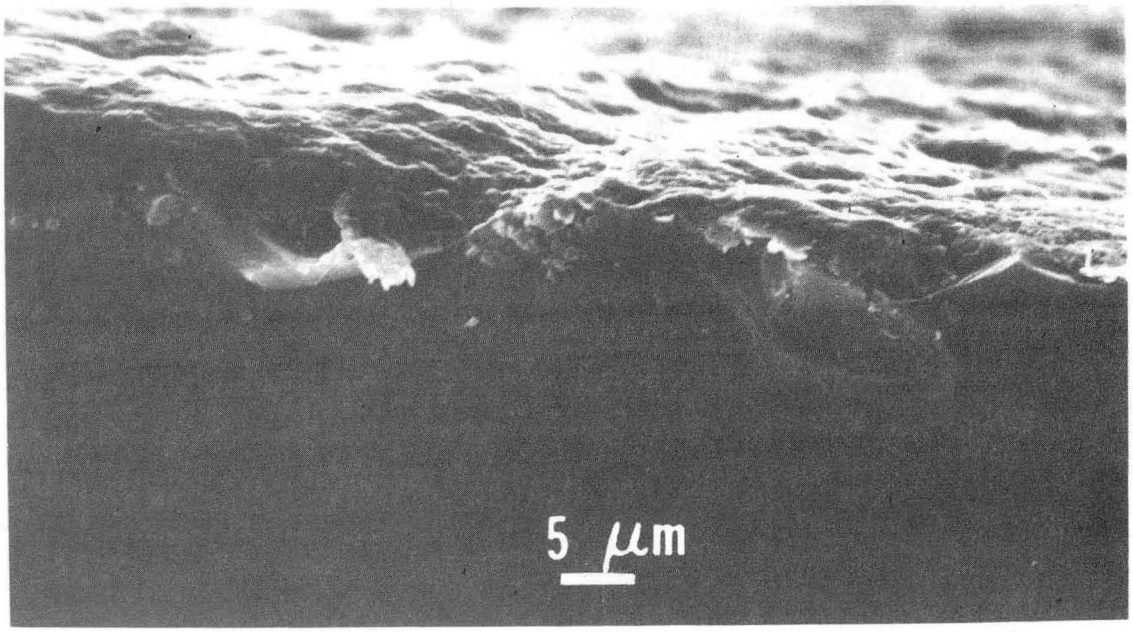

XBB 850-9215

Fig. 21

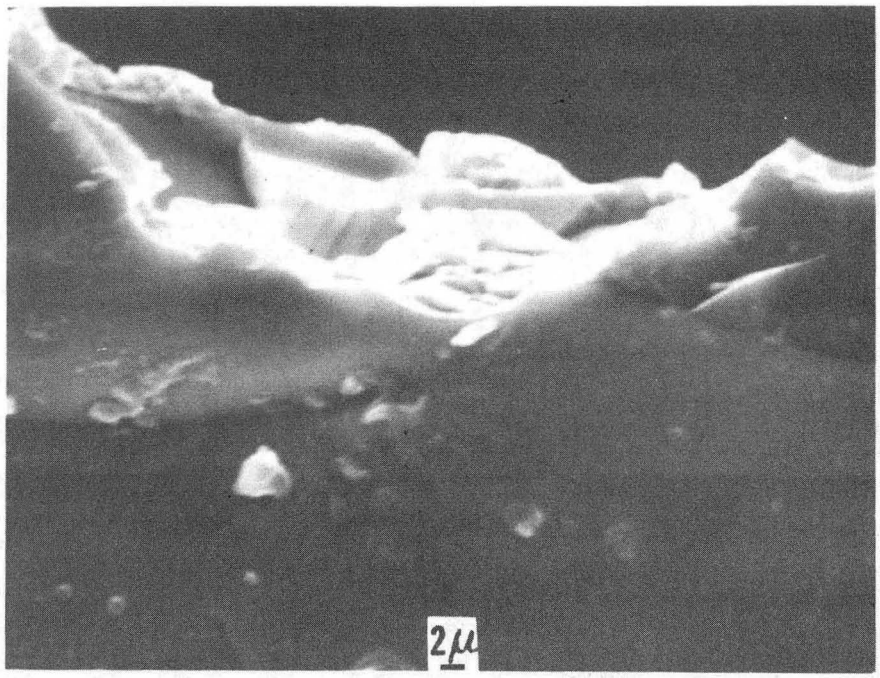

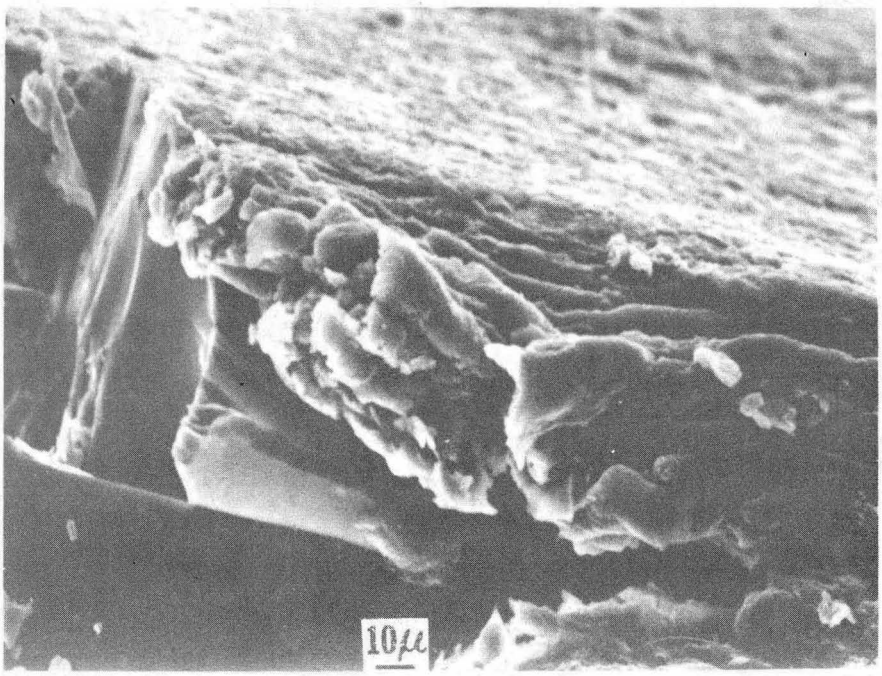

XBB 854-2574-A

Fig. 22

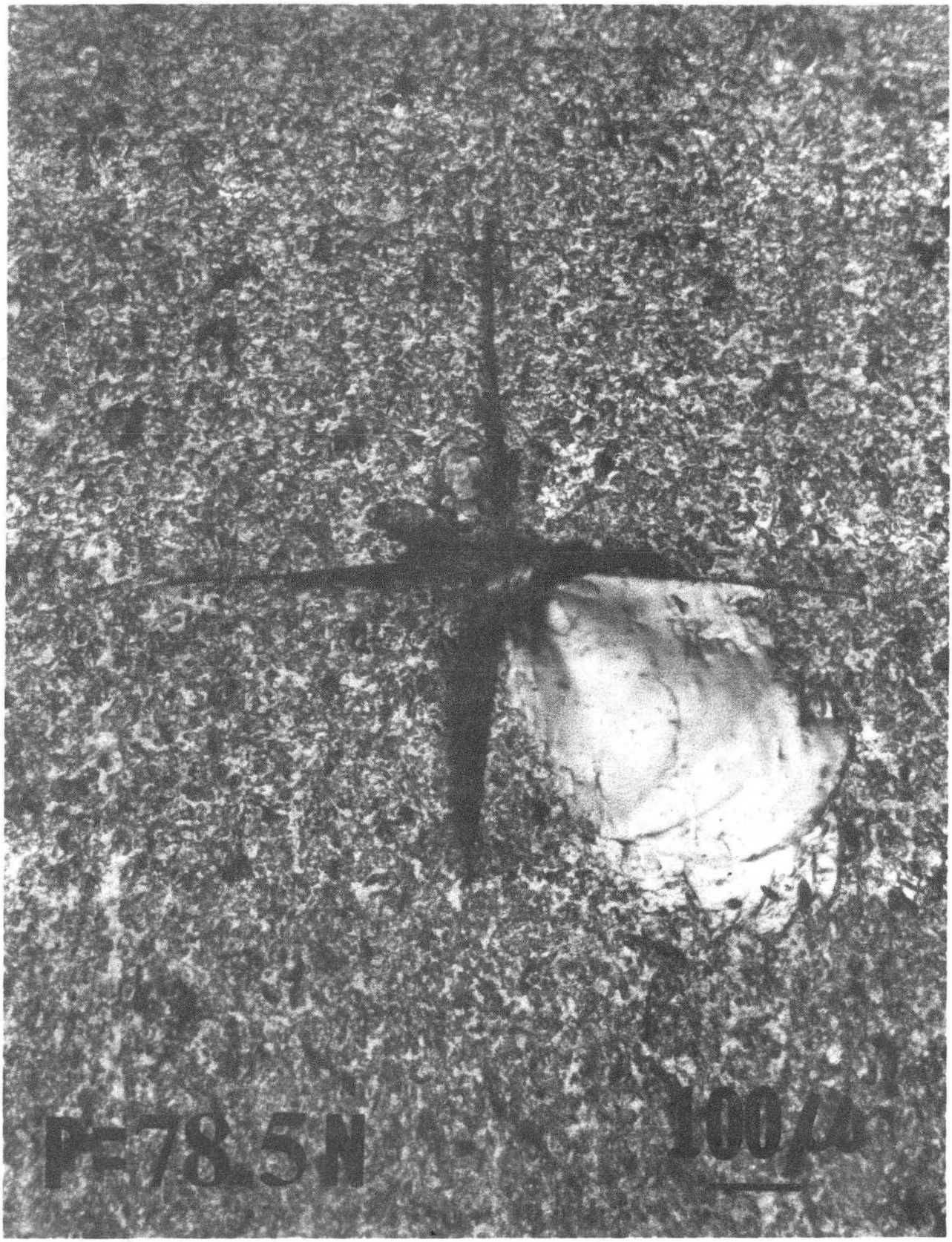

XBB 855-3963

Fig. 23

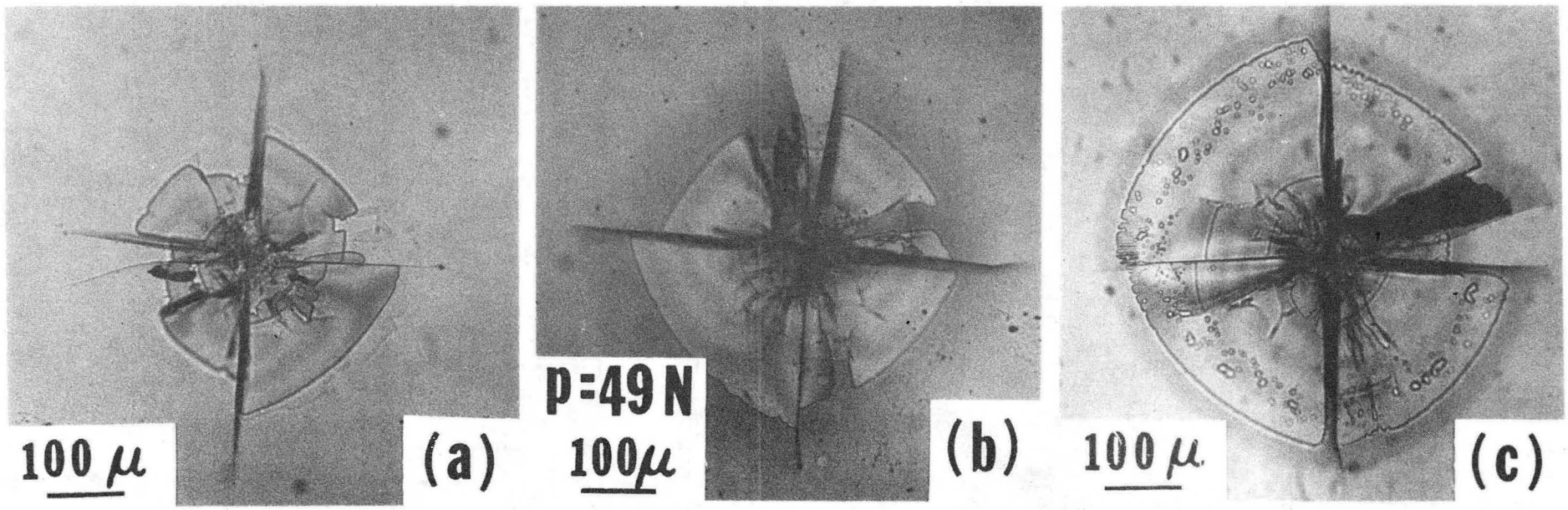

XBB 858-6932

Fig. 24

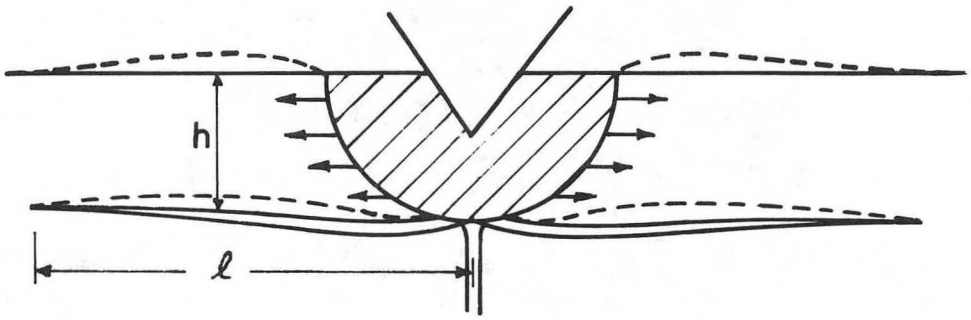

(a) As-received surface

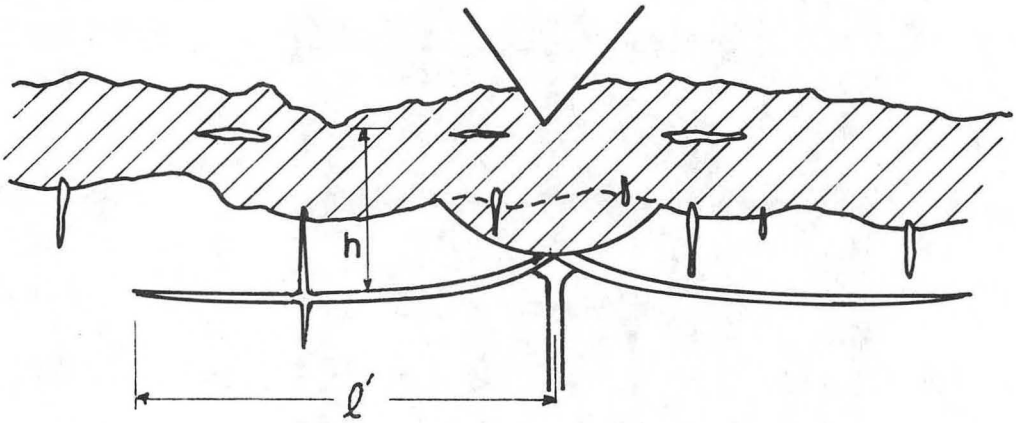

(b) Machined surface

XBL 859-6607

Fig. 25

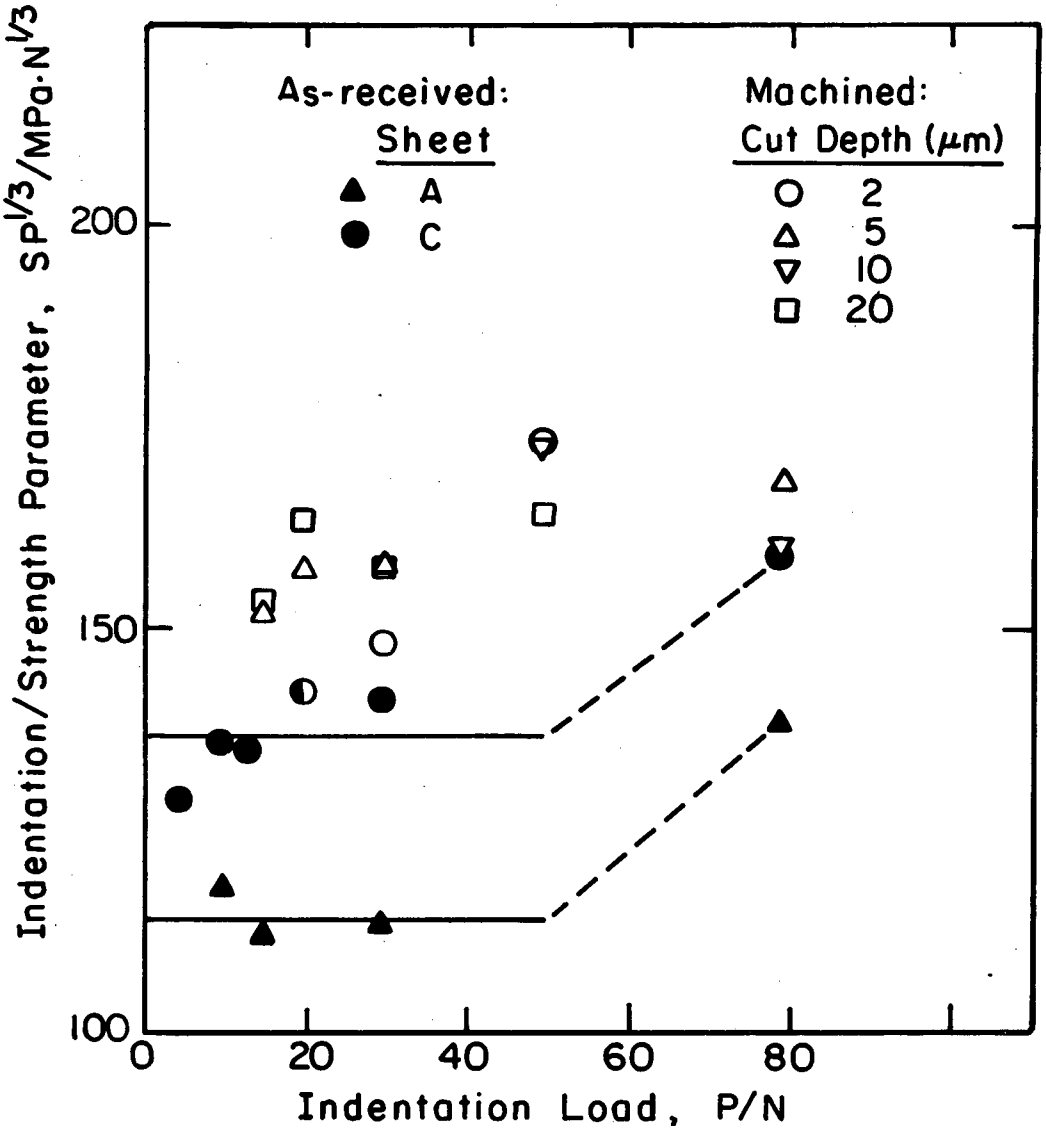

XBL 859-6608

Fig. 26

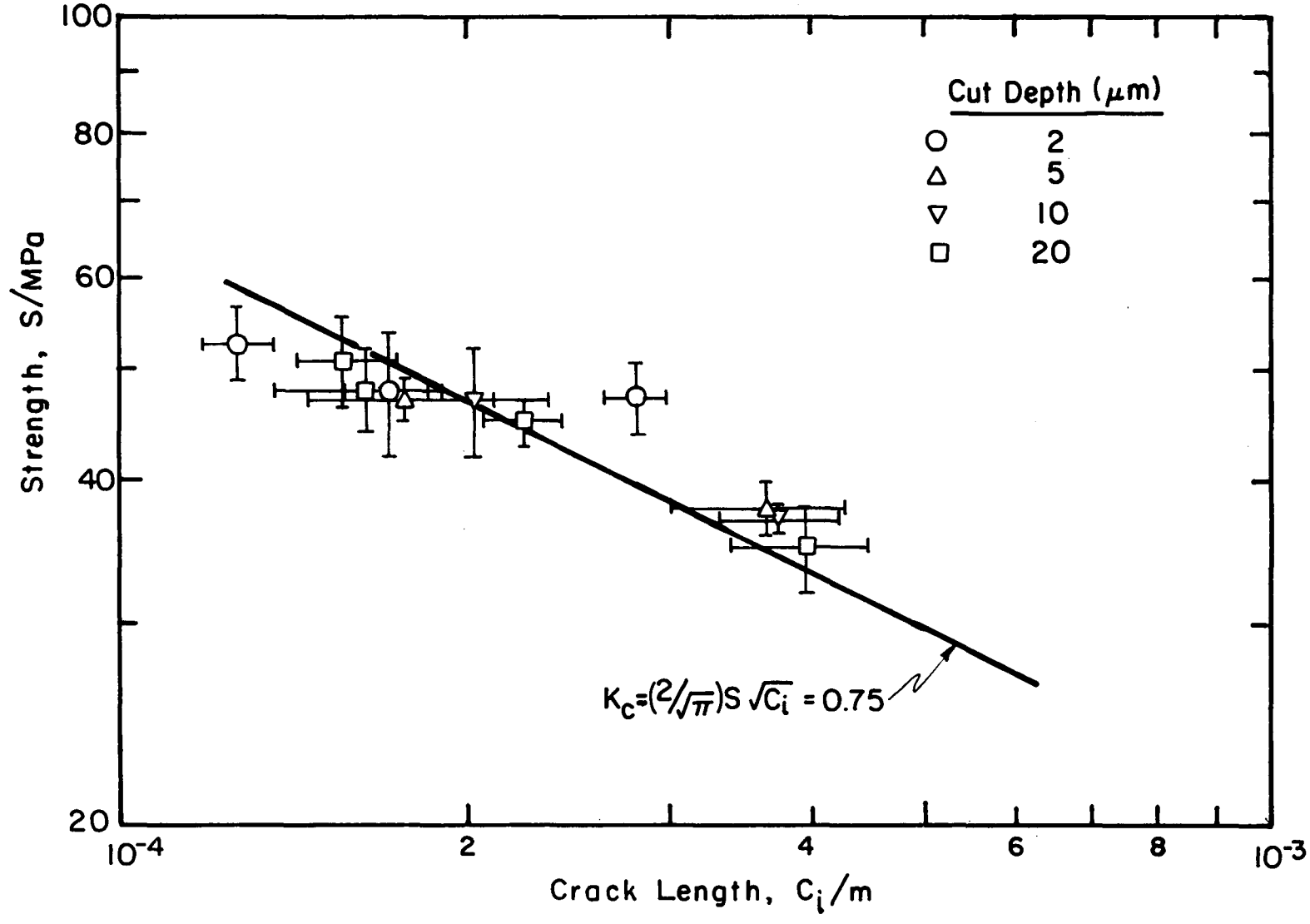

Fig. 27

XBL 859-3808

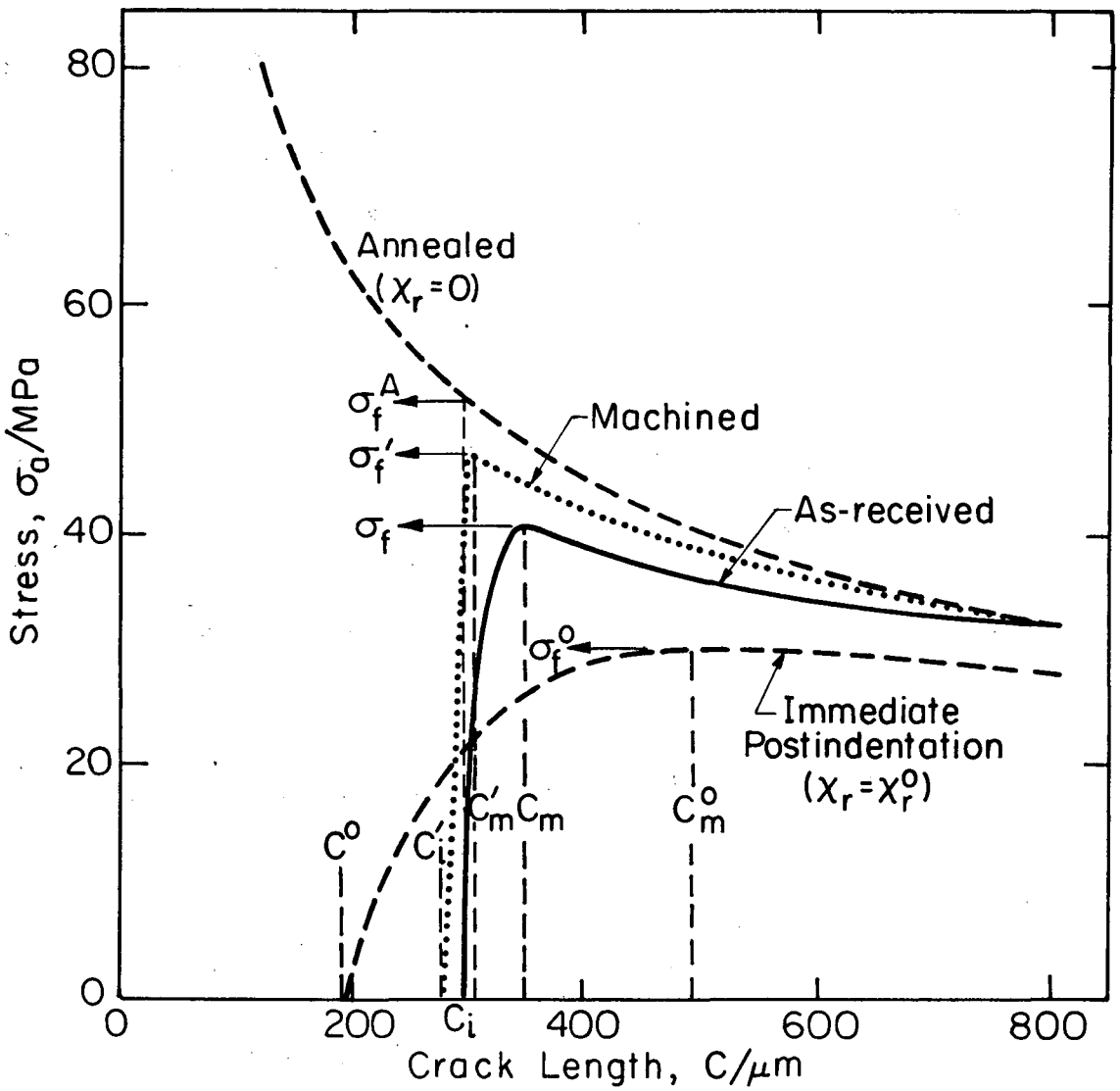

XBL 853-6009B

Fig. 28

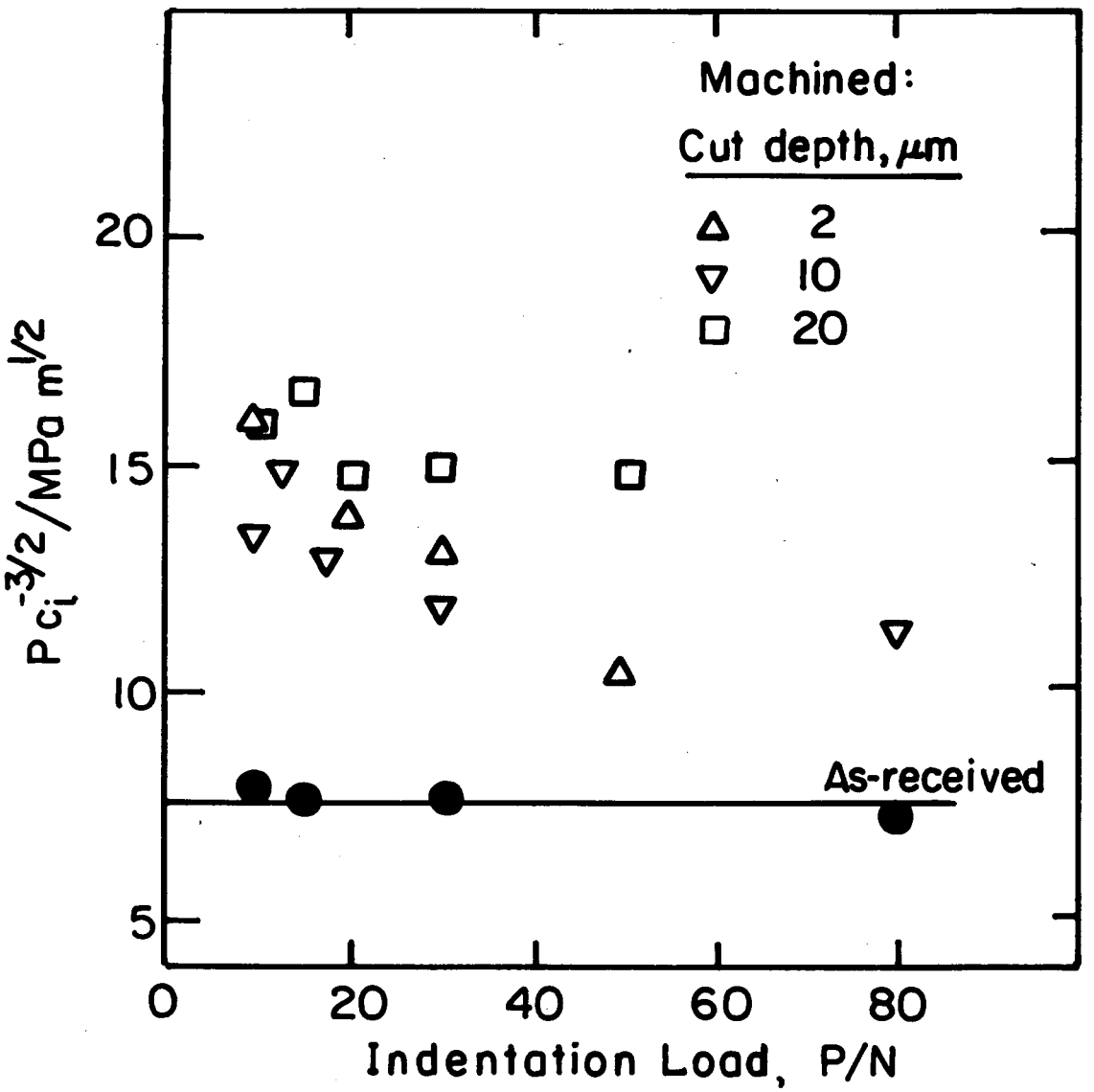

Fig. 29

XBL 859-6630

This report was done with support from the Department of Energy. Any conclusions or opinions expressed in this report represent solely those of the author(s) and not necessarily those of The Regents of the University of California, the Lawrence Berkeley Laboratory or the Department of Energy.

Reference to a company or product name does not imply approval or recommendation of the product by the University of California or the U.S. Department of Energy to the exclusion of others that may be suitable.

LAWRENCE BERKELEY LABORATORY
TECHNICAL INFORMATION DEPARTMENT
UNIVERSITY OF CALIFORNIA
BERKELEY, CALIFORNIA 94720